Mathematics MSc Dissertation MMTHM038, 2022/23

Modelling Higher-Order Network Dynamics in Presence of Triadic Interactions

Jun Yamamoto, ID 220167073

Supervisor: Prof. Ginestra Bianconi

A thesis presented for the degree of
Master of Science in *Mathematics*

School of Mathematical Sciences
Queen Mary University of London

Declaration of original work

This declaration is made on September 6, 2023.

Student's Declaration: I, Jun Yamamoto, hereby declare that the work in this thesis is my original work. I have not copied from any other students' work, work of mine submitted elsewhere, or from any other sources except where due reference or acknowledgement is made explicitly in the text, nor has any part been written for me by another person.

Referenced text has been flagged by:

1. Using italic fonts, **and**
2. using quotation marks "...", **and**
3. explicitly mentioning the source in the text.

Acknowledgements

I am deeply grateful to Prof. Ginestra Bianconi for her exceptional guidance and invaluable mentorship throughout the course of my dissertation project. Her insightful advice, constructive feedback, and dedication to my academic growth have been instrumental. I am truly fortunate to have had the privilege of working under Ginestra's supervision.

I extend my sincere appreciation to Dr. Anthony Baptista for his generous assistance and collaborative spirit. His willingness to share knowledge, provide valuable consultations, and share codes greatly enriched the quality of this dissertation. His help has been indispensable in overcoming the challenges of my research.

I would like to express my heartfelt gratitude to my coursemates Ailsa, Anjali, Hyesung, Richard, and Theo. Your camaraderie and shared experiences have made my academic journey at QMUL memorable and rewarding. The support and meaningful interactions that we have shared will forever be cherished. I am proud to have been part of such an inspiring group.

The financial support from the ITO Foundation for International Education Exchange is sincerely acknowledged. Their generous scholarship has enabled me to study at QMUL while fully focussing on the modules and research.

Last but not least, I would like to express my deep gratitude to my parents and sister for their unwavering support, encouragement, and belief in me. Their understanding has provided the foundation upon which I have built my academic pursuits. For that, I am forever grateful.

Abstract

In the last 25 years, extensive research on complex networks has contributed significantly to our understanding of the structural and dynamic features exhibited by a wide range of systems. Nevertheless, there are certain phenomena that cannot be adequately explained using conventional network frameworks. In recent years, there has been a growing interest in investigating higher-order interactions involving three or more nodes as a means to elucidate these phenomena. Our primary focus lies in examining triadic interactions, wherein a third node has the ability to engage in either positive or negative interactions with an edge connecting two other nodes. Such interactions can be observed in the neural networks of human brains, as well as in the interrelationships between species within ecosystems.

This study proposes a model that captures the node dynamics on a network under the influence of triadic interactions. The primary objective is to investigate the effects of triadic interactions on the node dynamics. The model has been designed with the capability to enable or disable triadic interaction. The analytical solution for the stationary node states in the absence of triadic interactions is presented, and the impacts of triadic interactions are examined by comparing numerical results in the presence of triadic interactions with the analytical one in their absence.

The study evaluates triadic interactions on simple network structures with three nodes that serve as the fundamental subgraph structures of networks with triadic interactions. We propose conditional correlation coefficients as a measure that signals the existence of triadic interactions and demonstrate how the signs and magnitude of triadic interactions can be observed in conditional correlation coefficients.

Contents

Chapter 1

Introduction

A complex network is the representation of the underlying structure of a complex system by a network (or, mathematically, a graph)[1], which consists of a set of nodes (vertices) and a set of links (edges). With the explosion in available big data from technology, biology, and social science over the past 25 years, the interdisciplinary field of complex networks, i.e., network science, has grown into one of the most flourishing academic fields [AB02, New03, New18]. Network science originated in the 1999 paper by Barabási et al., which reported the scale-free property, i.e., the property that the distribution of degrees (the number of links connecting to a node) follows a power law with an exponent between two and three [BA99]. Before the discovery of the scale-free property, most network studies assumed a Poisson degree distribution of random graphs and failed to reproduce many intriguing phenomena present in various complex systems. However, the heterogeneity of the scale-free property, often combined with the small-world property that the characteristic path length of the network scales with the logarithm of the number of nodes, allows descriptions of rich and diverse structural and dynamical characteristics of complex networks, such as robustness, epidemic spreading, and synchronisation [AB02, New03, BLM$^+$06, LNR17, New18].

Although network representations have largely succeeded and thrived as effec-

[1]In this work, we use the term 'network' and 'graph' interchangeably. Similarly, we also use 'nodes' and 'vertices', 'links', and 'edges' interchangeably.

tive ways of studying various complex systems, it was clear by the early 2010s that single-layer networks are not optimal for some systems with more than one type of interaction [Bia18]. For example, a power grid consists of a physical network of electric cables connecting power plants and houses and a wireless network of control units of the power plants that regulate the amount of electricity generated. In this case, the bi-layer representation with one layer representing the transmission network and another representing the control network seems more suitable, and in fact, is used to analyse the devastating blackout in Italy in 2003 [PM13]. To address this limitation of the single-layer representation, multi-layer networks have become a frequently used generalisation of networks. In the past decade, comprehensive studies have been conducted and a wide range of structural and dynamic characteristics, such as cascades, epidemic spread, and opinion dynamics, are well understood within the multi-layer network framework [BBC+14, KAB+14, Bia18]. In addition to multi-layer networks, various extensions, including temporal networks, weighed and directed networks, and spatial networks, have been actively studied over the last decade [ML16, HS19, New18].

Nearly 25 years of research on complex networks has advanced our understanding of the structural or dynamic features of diverse complex systems, but there exist many phenomena that still cannot be well described within the conventional frameworks. For example, explosive transitions in networks have been reported in various dynamics, and models with such transitions have been developed and studied intensively [DGGNA19], but these models incorporate very arbitrary and seemingly unnatural rules in their models [BAB+21]. To explain phenomena that are unnatural to describe conventionally or those that cannot be explained at all by conventional representations, the description as networks incorporating higher-order interactions consisting of three or more nodes, i.e., higher-order networks representation, has attracted much attention in recent years [BCI+20, BAB+21, Bia21].

In higher-order networks, interactions of three or more elements are described, for example, by hyperedges or simplicial complexes. Only a few years have passed since these description methods have become popular, but rapid progress has been made in understanding the structure and dynamics in the presence of higher-order interactions [BCI+20, BAB+21, Bia21]. In particular, the explosive transitions on the network mentioned earlier appear simply by introducing three-body interactions, without any additional unnatural rules [BAB+21]. Exploring complex systems as higher-order networks is promising because it is likely to provide a new framework for understanding structural and dynamic phenomena of networked systems.

It is, however, essential to note that there are many types of higher-order interactions, even if they are simply referred to as higher-order interactions. For example, in a coauthorship relationship between three researchers, there can be a relationship in which three researchers with close competence contribute equally (as in an equilateral triangle), a relationship in which the power balance among three is uneven (e.g., a student, a postdoc, and a supervisor), and a (directed) relationship in which a third person gets involved in the joint research of two researchers later in the form of advice and criticism. When describing a system as a higher-order network, it is necessary to apply an appropriate representation in accordance with the nature of the system.

This work considers a triadic interaction in which a third node interacts with the interaction between the two other nodes, as in the third case of the previous coauthorship examples. Such interactions are known, for example, in neuronal networks in the brain, where the synapses that fire between two neurones are inhibited or activated by another neural cell, called glia [CBL16]. As another example, there are reports that a third species interferes with an interaction between two other species in ecosystems [BKK16, GBMSA17, LS19]. While reports of triadic interactions exist in real systems, a general framework to describe triadic interactions is new and has yet to be fully developed and understood. In 2023, Sun et al. considered the percolation problem of networks in the presence of signed triadic interactions and reported that chaotic behaviours of the giant component size emerge [SRKB23]. Their findings hint that many more interesting phenomena can arise from triadic interactions. However, there is currently no comprehensive, general study examining how triadic interactions affect node dynamics on the network. Understanding how triadic interactions affect the node dynamics of a network would be of importance, for example, in order to examine whether it is possible to detect the existence of previously unexplored triadic interactions in multivariate timeseries data of node dynamics that have been measured from real systems.

In this study, a model of node dynamics on the network in the presence of triadic interactions is devised, and the relationship between the triadic interactions and the time evolution of node states in the dynamics is examined. The model is designed in a way that one can switch the triadic interaction on and off. In particular, we solve the stationary solution in the absence of triadic interactions analytically and then attempt to clarify how the presence of triadic interactions affects the node dynamics by comparing the numerical results with triadic interactions with the analytical result without triadic interactions. By specifically considering the dynamics in the simple network structures with three nodes that serve as the basic subgraph structures of any network with triadic interactions, we evaluate how and to what extent the triadic interactions on the three types of unit structures appear in the node dynamics. To this end, we propose conditional correlation coefficients as a measure to show the existence of triadic interactions, and we demonstrate from the examples that the signs and magnitude of triadic interactions can be detected from conditional correlation coefficients.

Finally, the structure of this dissertation is as follows: in Chap. 2, the mathematical facts used in the model and the analytical calculations are briefly summarised. In particular, the definition and properties of the multivariate Gaussian distribution are provided, followed by a summary of stochastic differential equations and their equivalence to the Fokker-Planck equations. In Chap. 3, the triadic interactions and the node dynamics incorporating triadic interactions are defined. Chapter 4 summarises the analytical and numerical results of the node dynamics model. Finally, Chap. 5 presents the conclusions.

Chapter 2

Background

Here we briefly introduce some mathematical preliminaries that will be used in later chapters. We start by presenting the definitions of networks and graph Laplacian in Sect. 2.1. Section 2.2 introduces the multivariate Gaussian distribution and some of its properties which we use in Chap. 4. Next, we discuss in Sect. 2.3 stochastic differential equations (SDEs) and show their equivalence to the Fokker-Planck equations (FPEs).

2.1 Networks and Graph Laplacian

We briefly introduce the definitions of networks and graph Laplacians, which will appear in our model of node dynamics defined in Chap. 3. For details, refer to standard textbooks or reviews on complex networks (or graph theory), such as [AB02, New03, LNR17, New18].

Definition 2.1.1. (undirected network; [New18]) Let $\mathcal{V}$ be a (nonempty) set of distinct elements, and let $\mathcal{E}$ be a set of distinct unordered pairs of elements in $\mathcal{V}$. Then, the undirected network (or graph) is defined by the ordered pair $(\mathcal{V}, \mathcal{E})$. The sets $\mathcal{V}$ and $\mathcal{E}$ are called the set of nodes (or vertices) and the set of links (or edges), respectively.

Definition 2.1.2. (adjacency matrix; [New18]) The adjacency matrix $\mathbf{A}$ of network $G = (\mathcal{V}, \mathcal{E})$ with $|\mathcal{V}| = N$ nodes is an $N \times N$ matrix whose (i, j)-th entry $(i, j \in \{1, \dots, N\})$ is defined by

$$A_{ij} = \begin{cases} 1 & \text{if } [i, j] \in \mathcal{E}, \\ 0 & \text{otherwise.} \end{cases} \tag{2.1.1}$$

Definition 2.1.3. (incidence matrix; [New18]) Let $G = (\mathcal{V}, \mathcal{E})$ be a network with $|\mathcal{V}| = N$ nodes and $|\mathcal{E}| = L$ links. The incidence matrix $\mathbf{B}$ of G is then defined by the $N \times L$ matrix whose (i, ℓ)-th entry $(i \in \{1, \dots, N\}$, $\ell \in \{1, \dots, L\})$ is defined by

$$B_{i\ell} = \begin{cases} -1 & \text{if } \ell = [i, j] \text{ and } i < j, \\ 1 & \text{if } \ell = [j, i] \text{ and } j < i, \\ 0 & \text{otherwise.} \end{cases} \tag{2.1.2}$$

Definition 2.1.4. (graph Laplacian; [New18]) Let $G = (\mathcal{V}, \mathcal{E})$ be a network with $|\mathcal{V}| = N$ nodes. The graph Laplacian $\mathbf{L}$ of $\mathcal{G}$ is an $N \times N$ matrix whose (i, j)-th entry $(i, j \in \{1, \dots, N\})$ is defined by

$$L_{ij} = \left(\mathbf{B}\mathbf{B}^\top\right)_{ij} = \begin{cases} \sum_{k=1}^{N} A_{ik} & \text{if } i = j, \\ -1 & \text{if } i \neq j \text{ and } [i, j] \in \mathcal{E}, \\ 0 & \text{otherwise,} \end{cases} \tag{2.1.3}$$

where $\mathbf{B}$ is the incidence matrix of G and A_{ij} is the (i, j)-th entry of the adjacency matrix $\mathbf{A}$ of G.

2.2 Multivariate Gaussian Distributions

Later in this work, we will deal with multivariate Gaussian distributions and will utilise some of their properties. We briefly review its definition and key properties. These are kept intentionally short; please refer to [Ton90, BN06, Hau16] for more details.

2.2.1 Definition

Let us first formally define the multivariate Gaussian distribution (or multivariate normal distribution).

Definition 2.2.1. (Multivariate Gaussian Distribution; [Ton90]) Let $\boldsymbol{X} \in \mathbb{R}^n$ be an n-dimensional random variable (where $n \in \mathbb{N}$). Then, $\boldsymbol{X}$ is said to follow the n-dimensional Gaussian distribution with mean vector $\boldsymbol{\mu} \in \mathbb{R}^n$ and covariance matrix $\boldsymbol{\Sigma} \in \mathbb{R}^{n\times n}$ if $\boldsymbol{\Sigma}$ is positive definite[1] and the joint probability density function $f_{\boldsymbol{X}}$ of $\boldsymbol{X}$ is given by

$$f_{\boldsymbol{X}}(\boldsymbol{x};\boldsymbol{\mu},\boldsymbol{\Sigma}) = \frac{1}{\sqrt{(2\pi)^n|\boldsymbol{\Sigma}|}} \exp\left[-\frac{1}{2}(\boldsymbol{x}-\boldsymbol{\mu})^\top \boldsymbol{\Sigma}^{-1}(\boldsymbol{x}-\boldsymbol{\mu})\right], \quad \boldsymbol{x} \in \mathbb{R}^n \qquad (2.2.1)$$

where $|\boldsymbol{\Sigma}|$ denotes the determinant of the covariance matrix $\boldsymbol{\Sigma}$. The random variable $\boldsymbol{X}$ is indicated by $\boldsymbol{X} \sim \mathcal{N}_n(\boldsymbol{\mu},\boldsymbol{\Sigma})$, or $\boldsymbol{X} \sim \mathcal{N}(\boldsymbol{\mu},\boldsymbol{\Sigma})$ if n is obvious. The probability density function $f_{\boldsymbol{X}}$ of $\boldsymbol{X} \sim \mathcal{N}_n(\boldsymbol{\mu},\boldsymbol{\Sigma})$ is denoted as $\mathcal{N}_n(\boldsymbol{X};\boldsymbol{\mu},\boldsymbol{\Sigma})$. The moment generating function of $\mathcal{N}_n(\boldsymbol{\mu},\boldsymbol{\Sigma})$ is defined as [Hau16]

$$M_{\boldsymbol{X}}(\tilde{\boldsymbol{t}}) = \exp\left[\tilde{\boldsymbol{t}}^\top \boldsymbol{\mu} + \frac{1}{2}\tilde{\boldsymbol{t}}^\top \boldsymbol{\Sigma}\tilde{\boldsymbol{t}}\right]. \qquad (2.2.2)$$

2.2.2 Properties

In the following subsections, we present a short list of important properties of multivariate Gaussian distribution that we shall use later.

2.2.2.1 Linear Transformation Theorem

Here we state and prove the linear transformation theorem which we use to derive the marginal and conditional probabilities for multivariate Gaussian distributions.

[1] By the definition of the covariance matrix $\boldsymbol{\Sigma}$, it is either positive definite or positive semi-definite. For simplicity, we limit our arguments to the cases in which $\boldsymbol{\Sigma}$ is positive definite throughout this work.

Theorem 2.2.1. (linear transformation theorem; [Ton90]) Let $\boldsymbol{X} \in \mathbb{R}^n$ be a random variable from a multivariate Gaussian distribution $\mathcal{N}(\boldsymbol{\mu}, \boldsymbol{\Sigma})$, and let $\boldsymbol{Y} \in \mathbb{R}^m$ be a linear transformation of $\boldsymbol{X}$ with

$$\boldsymbol{Y} = \mathbf{A}\boldsymbol{X} + \boldsymbol{b}, \tag{2.2.3}$$

where $\mathbf{A} \in \mathbb{R}^{m \times n}$ and $\boldsymbol{b} \in \mathbb{R}^m$ are constant matrices. Then the random variable $\boldsymbol{Y}$ follows a multivariate Gaussian distribution $\mathcal{N}(\mathbf{A}\boldsymbol{\mu} + \boldsymbol{b}, \mathbf{A}\boldsymbol{\Sigma}\mathbf{A}^\top)$.

Proof. [Soc20] Consider the moment generating function of $\boldsymbol{Y}$,

$$\begin{aligned} M_{\boldsymbol{Y}}(\boldsymbol{t}) &= \mathbb{E}\left[\exp\{\boldsymbol{t}^\top \boldsymbol{Y}\}\right] \\ &= \mathbb{E}\left[\exp\{\boldsymbol{t}^\top \mathbf{A}\boldsymbol{X}\}\right] \mathbb{E}\left[\exp\{\boldsymbol{t}^\top \boldsymbol{b}\}\right] \\ &= M_{\boldsymbol{X}}(\mathbf{A}^\top \boldsymbol{t}) \exp\left[\boldsymbol{t}^\top \boldsymbol{b}\right], \end{aligned} \tag{2.2.4}$$

where $\boldsymbol{t} \in \mathbb{R}^m$. Since the moment generating function of $\boldsymbol{X} \sim \mathcal{N}(\boldsymbol{\mu}, \boldsymbol{\Sigma})$ is given as Eq. (2.2.2), we can further rewrite $M_{\boldsymbol{Y}}(\boldsymbol{t})$ in Eq. (2.2.4) as

$$\begin{aligned} M_{\boldsymbol{Y}}(\boldsymbol{t}) &= \exp\left[\boldsymbol{t}^\top \mathbf{A}\boldsymbol{\mu} + \frac{1}{2}\boldsymbol{t}^\top \mathbf{A}\boldsymbol{\Sigma}\mathbf{A}^\top \boldsymbol{t}\right] \exp\left[\boldsymbol{t}^\top \boldsymbol{b}\right] \\ &= \exp\left[\boldsymbol{t}^\top (\mathbf{A}\boldsymbol{\mu} + \boldsymbol{b}) + \frac{1}{2}\boldsymbol{t}^\top \mathbf{A}\boldsymbol{\Sigma}\mathbf{A}^\top \boldsymbol{t}\right]. \end{aligned} \tag{2.2.5}$$

Therefore, $\boldsymbol{Y}$ follows the Gaussian distribution with mean vector $\mathbf{A}\boldsymbol{\mu} + \boldsymbol{b}$ and covariance matrix $\mathbf{A}\boldsymbol{\Sigma}\mathbf{A}^\top$. □

2.2.2.2 Marginal Distribution

Theorem 2.2.2. (Marginal distribution; [Ton90]) Let $\boldsymbol{X} \in \mathbb{R}^n$ be a random variable from multivariate Gaussian distribution $\mathcal{N}_n(\boldsymbol{\mu}, \boldsymbol{\Sigma})$. Let S be a subset of the indices of $\boldsymbol{X}$ and denote $s = |S|$. Define a subset vector $\boldsymbol{X}_S$ such that $\boldsymbol{X}_S = \mathbf{H}\boldsymbol{X}$, where $\mathbf{H}$ is an $s \times n$ matrix that maps the indices of $\boldsymbol{X}$ onto the indices of the subset vector

$\boldsymbol{X}_S$, i.e.,

$$H_{ij} = \begin{cases} 1 & \text{if } (X_s)_i = X_j, \\ 0 & \text{otherwise.} \end{cases} \tag{2.2.6}$$

Then, the marginal distribution of subset vector $\boldsymbol{X}_S$ follows $\mathcal{N}_s(\mathbf{H}\boldsymbol{\mu}, \mathbf{H}\boldsymbol{\Sigma}\mathbf{H}^\top)$.

Proof. Since $\mathbf{H}$ is a linear transformation, it follows directly from Theorem 2.2.1. □

2.2.2.3 Conditional Distribution

Theorem 2.2.3. (Conditional distribution; [Ton90]) Let $\boldsymbol{X} \in \mathbb{R}^n$ be a random variable from multivariate Gaussian distribution $\mathcal{N}_n(\boldsymbol{\mu}, \boldsymbol{\Sigma})$. For $k < n$, consider partions of $\boldsymbol{X}$, $\boldsymbol{\mu}$, and $\boldsymbol{\Sigma}$ such that

$$\boldsymbol{X} = \begin{pmatrix} \boldsymbol{X}_1 \\ \boldsymbol{X}_2 \end{pmatrix}, \quad \boldsymbol{\mu} = \begin{pmatrix} \boldsymbol{\mu}_1 \\ \boldsymbol{\mu}_2 \end{pmatrix}, \quad \boldsymbol{\Sigma} = \begin{pmatrix} \boldsymbol{\Sigma}_{11} & \boldsymbol{\Sigma}_{12} \\ \boldsymbol{\Sigma}_{21} & \boldsymbol{\Sigma}_{22} \end{pmatrix}, \tag{2.2.7}$$

where

$$\begin{aligned} \boldsymbol{X}_1 &= \begin{pmatrix} X_1 & X_2 & \cdots & X_k \end{pmatrix}^\top, \quad \boldsymbol{X}_2 = \begin{pmatrix} X_{k+1} & X_{k+2} & \cdots & X_n \end{pmatrix}^\top, \\ \boldsymbol{\mu}_1 &= \begin{pmatrix} \mu_1 & \mu_2 & \cdots & \mu_k \end{pmatrix}^\top, \quad \boldsymbol{\mu}_2 = \begin{pmatrix} \mu_{k+1} & \mu_{k+2} & \cdots & \mu_n \end{pmatrix}^\top. \end{aligned} \tag{2.2.8}$$

Then, the conditional distributions of $\boldsymbol{X}_1$ given $\boldsymbol{X}_2 = \boldsymbol{x}_2$ is multivariate Gaussian $\mathcal{N}_k(\boldsymbol{\mu}_{1\cdot 2}, \boldsymbol{\Sigma}_{11\cdot 2})$, where

$$\boldsymbol{\mu}_{1\cdot 2} = \boldsymbol{\mu}_1 + \boldsymbol{\Sigma}_{12}\boldsymbol{\Sigma}_{22}^{-1}(\boldsymbol{x}_2 - \boldsymbol{\mu}_2), \tag{2.2.9}$$

$$\boldsymbol{\Sigma}_{11\cdot 2} = \boldsymbol{\Sigma}_{11} - \boldsymbol{\Sigma}_{12}\boldsymbol{\Sigma}_{22}^{-1}\boldsymbol{\Sigma}_{21}. \tag{2.2.10}$$

Proof. The proof is omitted due to space constraints, but it can be found in Sect. 3.3.3 of [Ton90]. □

2.3 Stochastic Differential Equations and Fokker-Planck Equations

A stochastic differential equation (SDE) [Gar09, Oks13] takes the form:

$$dx(t) = a[t, x(t)]dt + b[t, x(t)]dW(t), \tag{2.3.1}$$

where $dW(t)$ is the differential form of the univariate standard Brownian motion. Similarly, a multivariate stochastic differential equation of $\boldsymbol{X}(t) \in \mathbb{R}^n$ takes the form:

$$d\boldsymbol{X}(t) = \boldsymbol{A}[t, \boldsymbol{X}(t)]dt + \mathbf{B}[t, \boldsymbol{X}(t)]d\boldsymbol{W}(t), \tag{2.3.2}$$

where $d\boldsymbol{W}(t)$ is the differential form of the n-dimensional standard Brownian motion and $\boldsymbol{A} \in \mathbb{R}^n$ and $\mathbf{B} \in \mathbb{R}^{n\times n}$ are coefficients.

Meanwhile, a Fokker-Planck equation (FPE) [RR96, Gar09] is a partial differential equation for probability density function $p(t, x)$ of random variable X. It takes the form:

$$\frac{\partial p(t,x)}{\partial t} = -\frac{\partial}{\partial x}\left[\mu(t,x)p(t,x)\right] + \frac{\partial^2}{\partial x^2}\left[D(t,x)p(t,x)\right]. \tag{2.3.3}$$

The multivariate version of an FPE is expressed as:

$$\frac{\partial p(t,\boldsymbol{X})}{\partial t} = -\sum_{i=1}^{n}\frac{\partial}{\partial X_i}\left[\mu_i(t,\boldsymbol{X})p(t,\boldsymbol{X})\right] + \frac{1}{2}\sum_{i=1}^{n}\sum_{j=1}^{n}\frac{\partial}{\partial X_i}\frac{\partial}{\partial X_j}\left[D_{ij}(t,\boldsymbol{X})p(t,\boldsymbol{X})\right], \tag{2.3.4}$$

where $\boldsymbol{X} \in \mathbb{R}^n$ is an n-dimensional vector.

In the following section, we define Itô's formula, which we apply to show the equivalence of SDEs and FPEs.

2.3.1 Itô's Formula

In order to show that SDEs of the form (2.3.1) are equivalent to the Fokker-Planck equations, we shall introduce Itô's formula.

Theorem 2.3.1. (multivariate Itô's formula; [Gar09])

$$\begin{aligned} df[\boldsymbol{X}(t)] = \Bigg\{ & \sum_i A_i[t, \boldsymbol{X}(t)] \frac{\partial}{\partial X_i} f[\boldsymbol{X}(t)] \\ & + \frac{1}{2} \sum_{i,j} \Big(\mathbf{B}[t, x(t)] \mathbf{B}^\top [t, \boldsymbol{X}(t)] \Big)_{ij} \frac{\partial}{\partial X_i} \frac{\partial}{\partial X_j} f[\boldsymbol{X}(t)] \Bigg\} dt \\ & + \sum_{i,j} B_{ij}[t, \boldsymbol{X}(t)] \frac{\partial}{\partial X_i} f[\boldsymbol{X}(t)] dW_i(t) \end{aligned} \tag{2.3.5}$$

Proof. (sketch; [Gar09]) Let f be an arbitrary twice-differentiable function of $\boldsymbol{X}(t)$. By the Taylor expansion of $df[\boldsymbol{X}(t)]$,

$$df[\boldsymbol{X}(t)] = \frac{\partial}{\partial t} f[\boldsymbol{X}(t)] dt + \left(\nabla f[\boldsymbol{X}(t)] \right)^\top d\boldsymbol{X}(t) + \frac{1}{2} \left(d\boldsymbol{X}(t) \right)^\top \left(\mathbf{H} f \right) \left(d\boldsymbol{X}(t) \right), \tag{2.3.6}$$

where $\mathbf{H}(f)$ is the Hessian matrix of the function f. Assuming $\frac{\partial}{\partial t} f[\boldsymbol{X}(t)] = 0$, and substituting Eq.(2.3.2) into Eq. (2.3.6), it follows that

$$\begin{aligned} df[\boldsymbol{X}(t)] = (\nabla f[\boldsymbol{X}(t)])^\top & \{\boldsymbol{A}[t, \boldsymbol{X}(t)]dt + \mathbf{B}[t, \boldsymbol{X}(t)]d\boldsymbol{W}(t)\} \\ & + \frac{1}{2} \{\boldsymbol{A}[t, \boldsymbol{X}(t)]dt + \mathbf{B}[t, \boldsymbol{X}(t)]d\boldsymbol{W}(t)\}^\top \\ & \times (\mathbf{H}f) \{\boldsymbol{A}[t, \boldsymbol{X}(t)]dt + \mathbf{B}[t, \boldsymbol{X}(t)]d\boldsymbol{W}(t)\} \\ = & \sum_i A_i[t, \boldsymbol{X}(t)] \frac{\partial}{\partial X_i} f[\boldsymbol{X}(t)]dt + \sum_{i,j} B_{ij}[t, \boldsymbol{X}(t)]dW_j(t) \frac{\partial}{\partial X_i} f[\boldsymbol{X}(t)]dt \\ & + \frac{1}{2} \sum_{i,j} \left(A_i[t, \boldsymbol{X}(t)]dt + \sum_k B_{ki}[t, \boldsymbol{X}(t)]dW_k(t) \right) \\ & \times \frac{\partial^2 f[\boldsymbol{X}(t)]}{\partial X_i \partial X_j} \left(A_j[t, \boldsymbol{X}(t)]dt + \sum_k B_{jk}[t, \boldsymbol{X}(t)]dW_k(t) \right). \end{aligned} \tag{2.3.7}$$

The right hand side of Eq. (2.3.7) further simplifies to

$$\begin{aligned} df[\boldsymbol{X}(t)] = & \sum_i A_i[t, \boldsymbol{X}(t)] \frac{\partial}{\partial X_i} f[\boldsymbol{X}(t)]dt + \sum_{i,j} B_{ij}[t, \boldsymbol{X}(t)]dW_j(t) \frac{\partial}{\partial X_i} f[\boldsymbol{X}(t)]dt \\ & + \frac{1}{2} \sum_{i,j} \Bigg\{ A_i[t, \boldsymbol{X}(t)] A_j[t, \boldsymbol{X}(t)]dt^2 \\ & \quad + A_i[t, \boldsymbol{X}(t)] \sum_k B_{ki}[t, \boldsymbol{X}(t)]dW_k(t)dt \\ & \quad + A_j[t, \boldsymbol{X}(t)]dt \sum_k B_{jk}[t, \boldsymbol{X}(t)]dW_k(t)dt \\ & \quad + \sum_k B_{ik}[t, \boldsymbol{X}(t)] B_{kj}[t, \boldsymbol{X}(t)]dW_i(t)dW_j(t) \Bigg\} \frac{\partial^2 f}{\partial X_i \partial X_j}. \end{aligned} \tag{2.3.8}$$

Using the relations $dt^2 \to 0$, $dtdW_i(t) \to 0$ and $dW_i^2(t) \to dt$ as $t \to \infty$ by the properties of multivariate Brownian motions[Gar09, Oks13], we arrive at

$$\begin{aligned} df[\boldsymbol{X}(t)] &= \sum_i A_i[t, \boldsymbol{X}(t)] \frac{\partial}{\partial X_i} f[\boldsymbol{X}(t)] dt + \sum_{i,j} B_{ij}[t, \boldsymbol{X}(t)] dW_j(t) \frac{\partial}{\partial X_i} f[\boldsymbol{X}(t)] dt \\ &\quad + \frac{1}{2} \sum_{i,j} \left(\mathbf{B}[t, \boldsymbol{X}(t)] \mathbf{B}^\top [t, \boldsymbol{X}(t)]\right)_{ij} \frac{\partial}{\partial X_i} \frac{\partial}{\partial X_j} f[\boldsymbol{X}(t)] dt \\ &= \Bigg\{ \sum_i A_i[t, \boldsymbol{X}(t)] \frac{\partial}{\partial X_i} f[\boldsymbol{X}(t)] \\ &\quad + \frac{1}{2} \sum_{i,j} \Big(\mathbf{B}[t, \boldsymbol{X}(t)] \mathbf{B}^\top [t, \boldsymbol{X}(t)]\Big)_{ij} \frac{\partial}{\partial X_i} \frac{\partial}{\partial X_j} f[\boldsymbol{X}(t)] \Bigg\} dt \\ &\quad + \sum_{i,j} B_{ij}[t, \boldsymbol{X}(t)] \frac{\partial}{\partial X_i} f[\boldsymbol{X}(t)] dW_i(t). \end{aligned} \tag{2.3.9}$$

Thus, we derived the multivariate Itô's formula (2.3.5). □

2.3.2 Equivalence to Fokker-Planck Equation

Here we present the proof sketch from [Gar09] to show the equivalence of SDEs of the form (2.3.2) and FPEs of the form (2.3.4). Let f be an arbitrary twice-differentiable function of $\boldsymbol{X}$. From the multivariate Itô's formula (2.3.5), the time derivative of $f(\boldsymbol{X}(t))$ is given by

$$\frac{\partial f(\boldsymbol{X})}{\partial t} = \sum_i A_i(t, \boldsymbol{X}) \frac{\partial}{\partial X_i} f(\boldsymbol{X}) + \frac{1}{2} \sum_{i,j} \Big(\mathbf{B}(t, \boldsymbol{X}) \mathbf{B}^\top (t, \boldsymbol{X})\Big)_{ij} \frac{\partial}{\partial X_i} \frac{\partial}{\partial X_j} f(\boldsymbol{X}). \tag{2.3.10}$$

The time derivative of the expectation value of $f(\boldsymbol{X})$ over $\boldsymbol{X}$ reads

$$\begin{aligned} \frac{\partial}{\partial t} \langle f(\boldsymbol{X}) \rangle &= \frac{\partial}{\partial t} \int f(\boldsymbol{X}) \Big[p(t, \boldsymbol{X} \mid t_0, \boldsymbol{X}_0)\Big] d\boldsymbol{X} \\ &= \int f(\boldsymbol{X}) \frac{\partial}{\partial t} \Big[p(t, \boldsymbol{X} \mid t_0, \boldsymbol{X}_0)\Big] d\boldsymbol{X}, \end{aligned} \tag{2.3.11}$$

as we can swap the order of the space integration and the time derivative.

The space average of the right hand side of Eq. (2.3.10) reads

$$
\begin{aligned}
&\left\langle \sum_i A_i(t,\boldsymbol{X}) \frac{\partial}{\partial X_i} f(\boldsymbol{X}) + \frac{1}{2} \sum_{i,j} \Big(\mathbf{B}(t,\boldsymbol{X}) \mathbf{B}^\top(t,\boldsymbol{X}) \Big)_{ij} \frac{\partial}{\partial X_i} \frac{\partial}{\partial X_j} f(\boldsymbol{X}) \right\rangle \\
&= \int d\boldsymbol{X} \left\{ \sum_i A_i(t,\boldsymbol{X}) \frac{\partial}{\partial X_i} f(\boldsymbol{X}) \right. \\
&\qquad \left. + \frac{1}{2} \sum_{i,j} \Big(\mathbf{B}(t,\boldsymbol{X}) \mathbf{B}^\top(t,\boldsymbol{X}) \Big)_{ij} \frac{\partial}{\partial X_i} \frac{\partial}{\partial X_j} f(\boldsymbol{X}) \right\} p(t, \boldsymbol{X}(t) \mid t_0, \boldsymbol{X}_0)
\end{aligned}
\tag{2.3.12}
$$

Integrating by parts, it follows that

$$
\begin{aligned}
&\left\langle \sum_i A_i(t,\boldsymbol{X}) \frac{\partial}{\partial X_i} f(\boldsymbol{X}) + \frac{1}{2} \sum_{i,j} \Big(\mathbf{B}(t,\boldsymbol{X}) \mathbf{B}^\top(t,\boldsymbol{X}) \Big)_{ij} \frac{\partial}{\partial X_i} \frac{\partial}{\partial X_j} f(\boldsymbol{X}) \right\rangle \\
&= - \int d\boldsymbol{X} f(\boldsymbol{X}) \sum_i \frac{\partial}{\partial X_i} \Big[A_i(t,\boldsymbol{X}) p(t, \boldsymbol{X}(t) \mid t_0, \boldsymbol{X}_0) \Big] \\
&\qquad + \frac{1}{2} \int d\boldsymbol{X} f(\boldsymbol{X}) \sum_{i,j} \frac{\partial}{\partial X_i} \frac{\partial}{\partial X_j} \left[\Big(\mathbf{B}(t,\boldsymbol{X}) \mathbf{B}^\top(t,\boldsymbol{X}) \Big)_{ij} p(t, \boldsymbol{X}(t) \mid t_0, \boldsymbol{X}_0) \right],
\end{aligned}
\tag{2.3.13}
$$

which further simplifies to

$$
\begin{aligned}
&\left\langle \sum_i A_i(t,\boldsymbol{X}) \frac{\partial}{\partial X_i} f(\boldsymbol{X}) + \frac{1}{2} \sum_{i,j} \Big(\mathbf{B}(t,\boldsymbol{X}) \mathbf{B}^\top(t,\boldsymbol{X}) \Big)_{ij} \frac{\partial}{\partial X_i} \frac{\partial}{\partial X_j} f(\boldsymbol{X}) \right\rangle \\
&= \int d\boldsymbol{X} f(\boldsymbol{X}) \left\{ - \sum_i \frac{\partial}{\partial X_i} \Big[A_i(t,\boldsymbol{X}) p(t, \boldsymbol{X}(t) \mid t_0, \boldsymbol{X}_0) \Big] \right. \\
&\qquad \left. + \frac{1}{2} \sum_{i,j} \frac{\partial}{\partial X_i} \frac{\partial}{\partial X_j} \left[\Big(\mathbf{B}(t,\boldsymbol{X}) \mathbf{B}^\top(t,\boldsymbol{X}) \Big)_{ij} p(t, \boldsymbol{X}(t) \mid t_0, \boldsymbol{X}_0) \right] \right\}.
\end{aligned}
\tag{2.3.14}
$$

From Eqs. (2.3.11) and (2.3.13), we obtain

$$\frac{\partial}{\partial t}p(t,\boldsymbol{X}(t)\mid t_0,\boldsymbol{X}_0) = -\sum_i \frac{\partial}{\partial X_i}\Big[A_i(t,\boldsymbol{X})p(t,\boldsymbol{X}(t)\mid t_0,\boldsymbol{X}_0)\Big] + \frac{1}{2}\sum_{i,j}\frac{\partial}{\partial X_i}\frac{\partial}{\partial X_j}\left[\Big(\mathbf{B}(t,\boldsymbol{X})\mathbf{B}^\top(t,\boldsymbol{X})\Big)_{ij}p(t,\boldsymbol{X}(t)\mid t_0,\boldsymbol{X}_0)\right]. \tag{2.3.15}$$

Therefore, we have shown that the multi-dimensional stochastic differential equation is equivalent to the multi-dimensional Fokker-Planck equation.

2.3.3 Example: Ornstein Uhlenbeck Process

The stochastic differential equation for the n-dimensional Ornstein-Uhlenbeck process is as follows [Gar09]:

$$d\boldsymbol{X} = -\mathbf{K}\boldsymbol{X}(t)dt + \boldsymbol{\Gamma}d\boldsymbol{W}(t), \tag{2.3.16}$$

where $\mathbf{K}\in\mathbb{R}^{n\times n}$ and $\boldsymbol{\Gamma}\in\mathbb{R}^{n\times n}$ are constant matrices. The solution of Eq. (2.3.16) can be expressed as

$$\boldsymbol{X}(t) = \boldsymbol{X}(t_0) - \mathbf{K}\int_{t_0}^{t}\boldsymbol{X}(t')dt' + \boldsymbol{\Gamma}\int_{t_0}^{t}d\boldsymbol{W}(t'), \tag{2.3.17}$$

where the second integral is the multi-dimensional Itô integral. From Eq. (2.3.15), the equivalent Fokker-Planck equaiton is as follows:

$$\frac{\partial}{\partial t}p(t,\boldsymbol{X}(t)\mid t_0,\boldsymbol{X}_0) = -\sum_i \frac{\partial}{\partial X_i}\Big[(\mathbf{K}\boldsymbol{X})_i\, p(t,\boldsymbol{X}(t)\mid t_0,\boldsymbol{X}_0)\Big] + \frac{1}{2}\sum_{i,j}\frac{\partial}{\partial X_i}\frac{\partial}{\partial X_j}\left[\Big(\boldsymbol{\Gamma}\boldsymbol{\Gamma}^\top\Big)_{ij}p(t,\boldsymbol{X}(t)\mid t_0,\boldsymbol{X}_0)\right]. \tag{2.3.18}$$

At the equilibrium, the time-derivative of the conditionary probability $p_{\mathrm{st}}(\boldsymbol{X}\mid$

$t_0, \boldsymbol{X}_0)$ is zero, i.e.

$$\begin{aligned}
0 &= -\sum_i \frac{\partial}{\partial X_i}\Big[-(\mathbf{K}\boldsymbol{X})_i \; p_{\mathrm{st}}(\boldsymbol{X} \mid t_0, \boldsymbol{X}_0)\Big] \\
&\quad + \frac{1}{2}\sum_{i,j} \frac{\partial}{\partial X_i}\frac{\partial}{\partial X_j}\left[\left(\mathbf{\Gamma}\mathbf{\Gamma}^\top\right)_{ij} p_{\mathrm{st}}(\boldsymbol{X} \mid t_0, \boldsymbol{X}_0)\right] \\
&= \sum_i \frac{\partial}{\partial X_i}\bigg\{-(\mathbf{K}\boldsymbol{X})_i \; p_{\mathrm{st}}(\boldsymbol{X} \mid t_0, \boldsymbol{X}_0) \\
&\qquad + \frac{1}{2}\sum_j \frac{\partial}{\partial X_j}\left[\left(\mathbf{\Gamma}\mathbf{\Gamma}^\top\right)_{ij} p_{\mathrm{st}}(\boldsymbol{X} \mid t_0, \boldsymbol{X}_0)\right]\bigg\}.
\end{aligned} \tag{2.3.19}$$

Using the results presented in [Gar09, VP19], we obtain from Eq. (2.3.19) the stationary solution

$$p_{\mathrm{st}}(\boldsymbol{X} \mid t_0, \boldsymbol{X}_0) = \frac{1}{\sqrt{(2\pi)^n|\mathbf{\Sigma}|}} \exp\left[-\frac{1}{2}\boldsymbol{X}^\top \mathbf{\Sigma}^{-1}\boldsymbol{X}\right], \tag{2.3.20}$$

where $\mathbf{\Sigma}$ is obtained by

$$\mathbf{K}\mathbf{\Sigma} + \mathbf{\Sigma}\mathbf{K}^\top = \mathbf{\Gamma}\mathbf{\Gamma}^\top. \tag{2.3.21}$$

For the details of this derivation, please refer to [Gar09, VP19]. Note that the stationary solution is a multivariate Gaussian distribution with mean vector $\mathbf{0}$ and covariance matrix $\mathbf{\Sigma}$.

Chapter 3

Model

In this chapter, we define our model of the node dynamics on networks with triadic interactions. We first define the triadic interaction and then present the model of node dynamics on networks with triadic interactions. Finally, we show the three basic motifs, which we discuss in Chap. 4.

3.1 Triadic Interaction

Here, we define triadic interactions that we consider in this work.

Definition 3.1.1. (triadic interaction)
Let G be a simple network with a set $\mathcal{V}$ of $N = |\mathcal{V}|$ nodes and a set $\mathcal{E}$ of $L = |\mathcal{E}|$ links. Let $i \in \mathcal{V}$ and $\ell \in \mathcal{E}$. Then, the triadic interaction $K_{\ell i}$ is the interaction between node i and link ℓ, and is defined as follows:

$$K_{\ell i} = \begin{cases} -1 & \text{if node } i \text{ inhibits the interaction represented by link } \ell, \\ 1 & \text{if node } i \text{ activates the interaction represented by link } \ell, \\ 0 & \text{otherwise.} \end{cases} \tag{3.1.1}$$

If $K_{\ell i} = 1$, then node i is called a positive regulator of link ℓ. If $K_{\ell i} = -1$, then node i is called a negative regulator of link ℓ. Finally, the matrix $\mathbf{K} \in \{-1, 0, 1\}^{L \times N}$, whose

(ℓ, i)-entry is given by $K_{\ell i}$, is called the incidence matrix of the triadic interactions in G.

Remark. Note that node $i \in \mathcal{V}$ of graph $G = (\mathcal{V}, \mathcal{E})$ cannot be both positive and negative regulators of link ℓ simultaneously, but node i can be a positive regulator of link ℓ and a negative regulator of another link ℓ' ($\ell' \neq \ell$).

3.2 Node Dynamics

Using the formalism of triadic interactions defined in Sec. 3.1, we consider the following node dynamics of networks with triadic interactions.

Definition 3.2.1. (node dynamics of networks with triadic interactions).
Let G be a simple network with a set $\mathcal{V}$ of nodes and a set $\mathcal{E}$ of links. Denote $N = |\mathcal{V}|$ and $L = |\mathcal{E}|$. Let $\mathbf{K} \in \mathbb{R}^{L\times N}$ be the incidence matrix of the triadic interactions in G. Suppose that each node $i \in \mathcal{V}$ possesses node state $X_i \in \mathbb{R}$ and that the state vector $\boldsymbol{X} \in \mathbb{R}^N$ is governed by the stochastic differential equation of the form

$$d\boldsymbol{X} = -(\mathbf{L}^{(\mathrm{T})} + \alpha\mathbf{I})\boldsymbol{X}dt + \boldsymbol{\Gamma} d\boldsymbol{W}_t, \tag{3.2.1}$$

where $\alpha \in \mathbb{R}_+$, $\gamma_i \in \mathbb{R}_+$ is the i-th diagonal entry of diagonal matrix $\boldsymbol{\Gamma}$, and $d\boldsymbol{W}_t$ is the N-dimensional standard Brownian motion. The matrix $\mathbf{L}^{(\mathrm{T})} \in \mathbb{R}^{N\times N}$ is the triadic Laplacian whose entries are given by

$$L_{ij}^{(T)} = \begin{cases} -J_{ij}(\boldsymbol{X}) & \text{if} \quad i \neq j, \\ \displaystyle\sum_{k=1}^{N} J_{ik}(\boldsymbol{X}) & \text{if} \quad i = j, \end{cases} \tag{3.2.2}$$

where the matrix $\mathbf{J}$ is defined as

$$J_{ij}(\boldsymbol{X}) = \begin{cases} w_+\theta\left(\sum_{k=1}^{N} K_{\ell k}X_k - \hat{T}\right) + w_-\theta\left(\hat{T} - \sum_{k=1}^{N} K_{\ell k}X_k\right) & \text{if } \ell = [i,j] \in \mathcal{E}, \\ 0 & \text{if } \ell = [i,j] \notin \mathcal{E}. \end{cases} \tag{3.2.3}$$

Here, $w_+, w_- \in \mathbb{R}_+$ $(w_+ > w_-)$ are respectively the strength parameters of positive and negative triadic interactions, $\hat{T} \in \mathbb{R}$ is the threshold parameter, and $\theta(\cdot)$ is the Heaviside function.

Remark. Note the following:

- $J_{ij}(\boldsymbol{X}) = w_+$ if the sum of node states of nodes regulating link $[i,j]$ via triadic interactions is greater than the threshold $\hat{T}$, while $J_{ij}(\boldsymbol{X}) = w_-$ if the sum of node states of nodes regulating link $[i,j]$ via triadic interactions is less than $\hat{T}$.
- The triadic Laplacian $\mathbf{L}^{(\mathrm{T})}$ can be expressed in terms of the incidence matrix $\mathbf{B} \in \mathbb{R}^{N\times L}$ of the structural network G as

  $$\mathbf{L}^{(\mathrm{T})} = \mathbf{B}\mathbf{W}\mathbf{B}^\top, \tag{3.2.4}$$

  where $\mathbf{W} \in \mathbb{R}^{L\times L}$ denotes the diagonal matrix whose diagonal elements are $W_{[i,j],[i,j]} = J_{ij}(\boldsymbol{X})$.

3.3 Examples: 3 Basic Motifs

Although our model of node dynamics is quite general, we consider, for simplicity, the network motifs with triadic interactions shown in Fig. 3.3.1. This is because any triadic interaction in larger networks is, in principle, decomposable into the three motif structures since triadic interactions in larger networks are the superposition of the three. The graph Laplacians $\mathbf{L}_\mathrm{a}$, $\mathbf{L}_\mathrm{b}$, and $\mathbf{L}_\mathrm{c}$ of the three motif structures are

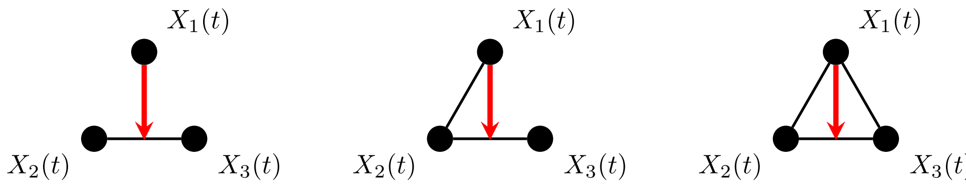

(a) G_{a} with $\mathbf{K}_{\mathrm{a}}$ (b) G_{b} with $\mathbf{K}_{\mathrm{b}}$ (c) G_{c} with $\mathbf{K}_{\mathrm{c}}$

Figure 3.3.1: Three network motifs with triadic interactions. In each network, the red arrow indicates the triadic interaction.

given by

$$\mathbf{L}_{\mathrm{a}} = \begin{pmatrix} 0 & 0 & 0 \\ 0 & 1 & -1 \\ 0 & -1 & 1 \end{pmatrix}, \quad \mathbf{L}_{\mathrm{b}} = \begin{pmatrix} 1 & -1 & 0 \\ -1 & 2 & -1 \\ 0 & -1 & 1 \end{pmatrix}, \quad \mathbf{L}_{\mathrm{c}} = \begin{pmatrix} 2 & -1 & -1 \\ -1 & 2 & -1 \\ -1 & -1 & 2 \end{pmatrix}. \quad (3.3.1)$$

The incidence matrix of the triadic interactions in the three motifs shown in Fig. 3.3.1 are as follows:

$$\text{motif (a): } \mathbf{K}_{\mathrm{a}}^{\pm} = \begin{pmatrix} \pm 1 & 0 & 0 \end{pmatrix}, \quad (3.3.2)$$

$$\text{motif (b): } \mathbf{K}_{\mathrm{b}}^{\pm} = \begin{pmatrix} 0 & 0 & 0 \\ \pm 1 & 0 & 0 \end{pmatrix}, \quad (3.3.3)$$

$$\text{motif (c): } \mathbf{K}_{\mathrm{c}}^{\pm} = \begin{pmatrix} 0 & 0 & 0 \\ 0 & 0 & 0 \\ \pm 1 & 0 & 0 \end{pmatrix}, \quad (3.3.4)$$

where $\pm$ indicates the signs of triadic interactions.

Chapter 4

Results

In this chapter, we present the analytical and numerical results for the node dynamics on networks with and without triadic interactions. In Sect. 4.1, we report the analytical results on the stationary node state distributions, covariances, and conditional correlations in the absence of triadic interactions. We first show the general results, and then present the examples from the three motifs structures from Sec. 3.3. These analytical results are confirmed by numerical simulations. In Sect. 4.2, we present the numerical results on the stationary node state distributions, covariances, and conditional correlations in the presence of triadic interactions. By comparing the results in the absence and presence of triadic interactions, we discuss the effects of triadic interactions on the node dynamics. We conclude in Sect. 4.3 by summarising the results and discussing the implications of the results.

4.1 In the Absence of Triadic Interactions

Before we begin our numerical investigations into the effects of triadic interactions on the node dynamics, it is instructive first to consider the case where triadic interactions are absent and then use these results to identify the effects of triadic interactions on the node dynamics. For this purpose, we present the analytical results on the stationary node state distributions, covariance matrix, and conditional correlations without triadic interactions. As we shall see, the analytical results in the absence of triadic interactions are very useful in understanding the effects of triadic interactions, since the analytical results are quite simple and intuitive. The natures of the analytical results enable us to identify the effects of triadic interactions when we introduce them.

Let $G = (\mathcal{V}, \mathcal{E})$ be a structural network consisting of node set $\mathcal{V}$ and link set $\mathcal{E}$. The node dynamics of the form (3.2.1) is exactly solvable in the absence of triadic interactions, i.e., if $K_{\ell i} = 0$ for $\forall \ell \in \mathcal{E}, i \in \mathcal{V}$. In fact, the stationary distribution p_{st} of node states $\boldsymbol{X}$ is an N-dimensional centred Gaussian distribution

$$p_{\mathrm{st}}(\boldsymbol{X}) = \frac{1}{\sqrt{(2\pi)^N |\boldsymbol{\Sigma}|}} \exp\left[-\frac{1}{2}\boldsymbol{X}^\top \boldsymbol{\Sigma}^{-1} \boldsymbol{X}\right], \tag{4.1.1}$$

with mean vector

$$\overline{\boldsymbol{X}} = \boldsymbol{0} \tag{4.1.2}$$

and covariance matrix

$$\boldsymbol{\Sigma} = \frac{\gamma^2}{2} \left(w_- \mathbf{L} + \alpha \mathbf{I}\right)^{-1}. \tag{4.1.3}$$

For interested readers, the derivation of the stationary distribution (4.1.1) is presented in Appendix A.

In order to characterise the triadic interactions, we compute the conditional correlation coefficients introduced by [Mau16].

Definition 4.1.1. (conditional correlation coefficient; [Mau16]) Let X and Y be random variables defined in the probability space $(\Omega, \mathcal{F}, P)$ and $\mathcal{A} \in \mathcal{F}$ such that $P(\mathcal{A}) > 0$. The conditional (Pearson) correlation coefficient $\rho(X, Y|\mathcal{A})$ is then defined by

$$\rho(X, Y|\mathcal{A}) = \frac{\mathbb{E}\left[(X - \mathbb{E}\left[X|\mathcal{A}\right])(Y - \mathbb{E}\left[Y|\mathcal{A}\right])|\mathcal{A}\right]}{\sqrt{\mathbb{E}\left[(X - \mathbb{E}\left[X|\mathcal{A}\right])^2|\mathcal{A}\right] \mathbb{E}\left[(Y - \mathbb{E}\left[Y|\mathcal{A}\right])^2|\mathcal{A}\right]}}, \tag{4.1.4}$$

where $0 \leq \rho(X, Y|\mathcal{A}) \leq 1$.

From the definition (4.1.4) and Theorem 2.2.2 and 2.2.3, we can show that the conditional correlation coefficient in our node dynamics is given as

$$\rho(X_i, X_j \mid X_k = \tilde{x}) = \frac{\Sigma_{ij} - \Sigma_{kk}^{-1}\Sigma_{ik}\Sigma_{kj}}{\sqrt{(\Sigma_{ii} - \Sigma_{kk}^{-1}\Sigma_{ik}\Sigma_{ki})(\Sigma_{jj} - \Sigma_{kk}^{-1}\Sigma_{jk}\Sigma_{kj})}}, \quad \tilde{x} \in \mathbb{R}. \tag{4.1.5}$$

The details of its derivation are shown in Appendix B. For convenience of notation, we sometimes denote it as $\rho_{ij|k}(\tilde{x})$. The conditional correlation coefficient in our node dynamics is independent of the values of the conditional variable X_k, if there are no triadic interactions in the network.

As mentioned in Sect. 3.3, we consider the effect of triadic interactions in the node dynamics on the three motifs shown in Fig. 3.3.1. Therefore, here we present the analytical forms of the stationary node state distribution, covariances, and conditional correlation coefficients for the three motifs in the absence of triadic interactions.

For motif G_a in Fig. 3.3.1(a) but without the triadic interaction indicated by the red arrow, we obtain the covariance matrix $\mathbf{\Sigma}_\mathrm{a}$ of G_a as

$$\mathbf{\Sigma}_\mathrm{a} = \frac{\gamma^2}{2\alpha(\alpha + 2w_-)} \begin{pmatrix} \alpha + 2w_- & 0 & 0 \\ 0 & \alpha + w_- & w_- \\ 0 & w_- & \alpha + w_- \end{pmatrix}, \tag{4.1.6}$$

from Eq. (4.1.3). Figure 4.1.1 shows the close agreement between the theoretical values of the covariances in Eq. (4.1.6) and the numerically computed covariances from 10^3 realisations of the node dynamics on motif (a).

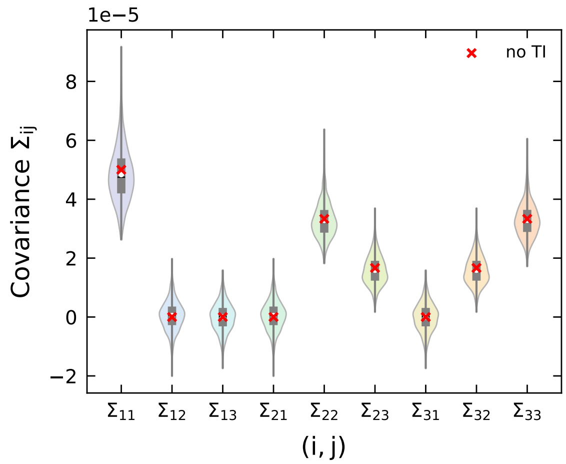

Figure 4.1.1: The covariance matrix $\mathbf{\Sigma}_{\mathrm{a}}$ of the network G_{a} without triadic interactions. The simulations are run with parameters $w_{-} = 1$, $w_{+} = 2$, $\alpha = 1$, $\hat{T} = 10^{-3}$, $\gamma = 10^{-2}$, $dt = 10^{-2}$, and $T_{\max} = 100$. The ticks on the horizontal axis represent the entries in the covariance matrix. The distributions of numerically computed covariances from 10^3 realisations (with time range $[T_{\max}/2, T_{\max}]$) are shown as box plots with the median (black line) and the mean (white circle). The colour-filled curves are the kernel density estimates of the distributions. The red crosses indicate the theoretical values of the covariances in Eq. (4.1.6).

From Eq. (4.1.1), the stationary solution of the joint PDF of node states in G_{a} is

$$\begin{aligned}
&p_{123}^{\mathrm{st}}(X_1, X_2, X_3) \\
&= \mathcal{N}_3\left(X_1, X_2, X_3; 0, \mathbf{\Sigma}_{\mathrm{a}}\right) \\
&= \left(\frac{1}{\pi\gamma^2}\right)^{\frac{3}{2}} \sqrt{\alpha^2(\alpha + 2w_{-})} \\
&\quad \times \exp\left[-\frac{1}{\gamma^2}\left\{\alpha X_1^2 + (\alpha + w_{-})(X_2^2 + X_3^2) - 2w_{-}X_2X_3\right\}\right].
\end{aligned} \tag{4.1.7}$$

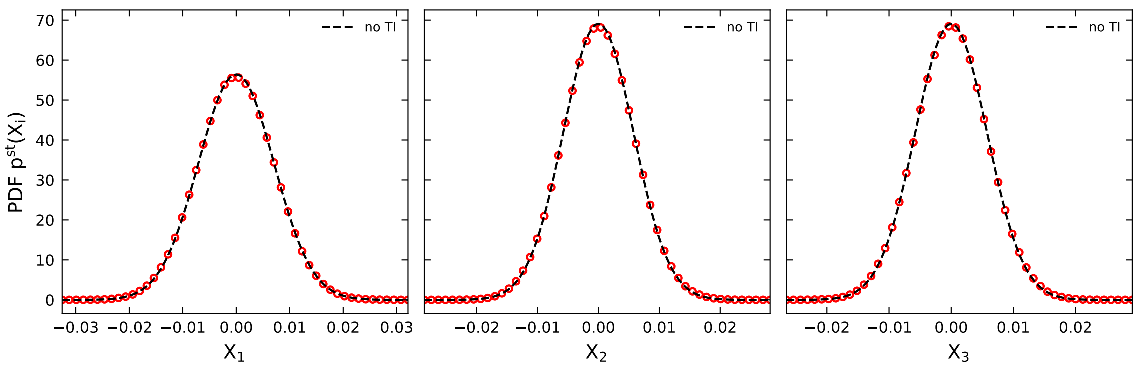

Figure 4.1.2: Stationary node state distribution of motif G_a without triadic interactions. The simulations are conducted with parameter values $w_- = 1$, $w_+ = 2$, $\alpha = 1$, $\hat{T} = 10^{-3}$, $\gamma = 10^{-2}$, $dt = 10^{-2}$, and $T_\mathrm{max} = 100$. The black dashed lines are the theoretical PDFs given by Eqs. (4.1.8)–(4.1.10), and the red open circles are the empirical marginal PDFs obtained from 10^3 realisations of the simulations. For each realisation, we extracted data from time range $[T_\mathrm{max}/2, T_\mathrm{max}]$. Empirical PDFs are obtained by binning the data points into 50 bins.

By applying Theorem 2.2.2, we derive the marginal PDFs of X_1, X_2, and X_3 as

$$p_1^{\mathrm{st}}(X_1) = \mathcal{N}_1\left(0, (\mathbf{\Sigma}_a)_{11}\right) = \sqrt{\frac{\alpha}{\pi\gamma^2}} \exp\left[-\frac{\alpha}{\gamma^2} X_1^2\right], \tag{4.1.8}$$

$$p_2^{\mathrm{st}}(X_2) = \mathcal{N}_1\left(X_2; 0, (\mathbf{\Sigma}_a)_{22}\right) = \sqrt{\frac{\alpha(\alpha+2w_-)}{\pi\gamma^2(\alpha+w_-)}} \exp\left[-\frac{1}{\gamma^2}\frac{\alpha(\alpha+2w_-)}{\alpha+w_-} X_2^2\right], \tag{4.1.9}$$

$$p_3^{\mathrm{st}}(X_3) = \mathcal{N}_1\left(X_3; 0, (\mathbf{\Sigma}_a)_{33}\right) = \sqrt{\frac{\alpha(\alpha+2w_-)}{\pi\gamma^2(\alpha+w_-)}} \exp\left[-\frac{1}{\gamma^2}\frac{\alpha(\alpha+2w_-)}{\alpha+w_-} X_3^2\right], \tag{4.1.10}$$

where $(\mathbf{\Sigma}_a)_{ij}$ denotes the (i, j)-th entry of the covariance matrix $\mathbf{\Sigma}_\mathrm{a}$. Equations (4.1.8)–(4.1.10) are confirmed by numerical simulations as shown in Fig. 4.1.2.

From Eqs. (4.1.6) and (4.1.5), the conditional correlations conditioned on $X_1 = \tilde{x}$,

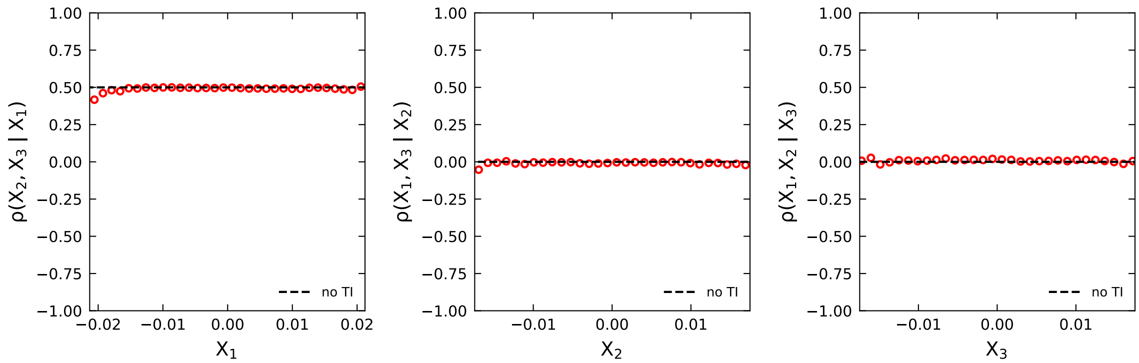

Figure 4.1.3: Conditional correlation coefficients in motif G_{a} without triadic interactions. The simulation parameters are set to $w_- = 1$, $w_+ = 2$, $\alpha = 1$, $\hat{T} = 10^{-3}$, $\gamma = 10^{-2}$, $dt = 10^{-2}$, and $T_{\max} = 100$. The black dashed line is the theoretical conditional correlation given by Eq. (4.1.5), and the red open circles are the empirical conditional correlations obtained from 10^3 realisations of the simulations, where we extracted data points from time range $[T_{\max}/2, T_{\max}]$. Empirical conditional correlations are obtained by binning the data points into 50 bins. Due to the small sample size, the empirical conditional correlations fluctuate at both ends of the conditional variable, and thus we restrict the plotting range to $[-3\sigma_k, 3\sigma_k]$, where σ_k ($k \in \{1, 2, 3\}$) is the standard deviation of the conditional variable X_k.

$X_2 = \tilde{x}$, $X_3 = \tilde{x}$ are respectively

$$\rho_{23|1} \equiv \rho(X_2, X_3 \mid X_1 = \tilde{x}) = \frac{w_-}{\alpha + w_-}, \tag{4.1.11}$$

$$\rho_{13|2} \equiv \rho(X_1, X_3 \mid X_2 = \tilde{x}) = 0, \tag{4.1.12}$$

$$\rho_{12|3} \equiv \rho(X_1, X_2 \mid X_3 = \tilde{x}) = 0. \tag{4.1.13}$$

Figure 4.1.3 visualises the conditional correlations $\rho_{23|1}(X_1)$, $\rho_{13|2}(X_2)$, and $\rho_{12|3}(X_3)$ from Eqs. (4.1.11)–(4.1.13) and the numerical values from 10^3 simulations of the node dynamics. The analytical and numerical results align mostly well, but we observe large fluctuations at both ends of the conditional variable. They are caused by the small sample sizes at both ends.

Next, for motif G_{b} in Fig. 3.3.1(b) without triadic interactions, the covariance

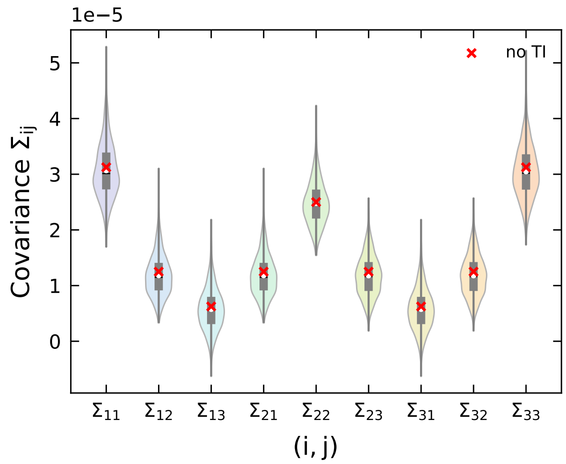

Figure 4.1.4: The covariance matrix $\mathbf{\Sigma}_{\mathrm{b}}$ of the network G_{b} without triadic interactions. The simulations are run with parameters $w_- = 1$, $w_+ = 2$, $\alpha = 1$, $\hat{T} = 10^{-3}$, $\gamma = 10^{-2}$, $dt = 10^{-2}$, and $T_{\max} = 100$. The ticks on the horizontal axis represent the entries in the covariance matrix. The distributions of numerically computed covariances from 10^3 realisations (with time range $[T_{\max}/2, T_{\max}]$) are shown as box plots with the median (black line) and the mean (white circle). The colour-filled curves are the kernel density estimates of the distributions. The red crosses indicate the theoretical values of the covariances in Eq. (4.1.14).

matrix $\mathbf{\Sigma}_{\mathrm{b}}$ of G_{b} reads

$$\begin{aligned}\mathbf{\Sigma}_{\mathrm{b}} = &\frac{\gamma^2}{2\alpha(\alpha+w_-)(\alpha+3w_-)} \\ &\times \begin{pmatrix} \alpha^2+3\alpha w_- + w_-^2 & w_-(\alpha+w_-) & w_-^2 \\ w_-(\alpha+w_-) & (\alpha+w_-)^2 & w_-(\alpha+w_-) \\ w_-^2 & w_-(\alpha+w_-) & \alpha^2+3\alpha w_- + w_-^2 \end{pmatrix},\end{aligned} \tag{4.1.14}$$

which follows from Eq. (4.1.3). The analytical form in Eq. (4.1.14) are confirmed by numerical simulations, as shown in Fig. 4.1.4.

From Eq. (4.1.1) and the covariance matrix in Eq. (4.1.14), the stationary solution of the joint PDF of node states in G_b is

$$\begin{aligned}
&p^{\mathrm{st}}_{123}(X_1, X_2, X_3) = \mathcal{N}_3(X_1, X_2, X_3; 0, \mathbf{\Sigma}_\mathrm{b}) \\
&= \left(\frac{1}{\pi\gamma^2}\right)^{\frac{3}{2}} \sqrt{\alpha(\alpha+w_-)(\alpha+3w_-)} \\
&\qquad \times \exp\left[-\frac{1}{\gamma^2}\left\{(\alpha+2w_-)X_2^2 + (\alpha+w_-)(X_1^2+X_3^2) - 2w_-X_2(X_1+X_3)\right\}\right].
\end{aligned} \tag{4.1.15}$$

By applying Theorem 2.2.2, we obtain the marginal PDFs of X_1, X_2, and X_3 as

$$\begin{aligned}
p^{\mathrm{st}}_1(X_1) &= \mathcal{N}_1(X_1; 0, (\mathbf{\Sigma}_\mathrm{b})_{11}) \\
&= \sqrt{\frac{\alpha(\alpha+w_-)(\alpha+3w_-)}{\pi\gamma^2(\alpha^2+3\alpha w_-+w_-^2)}} \exp\left[-\frac{1}{\gamma^2}\frac{\alpha(\alpha+w_-)(\alpha+3w_-)}{\alpha^2+3\alpha w_-+w_-^2}X_1^2\right], && (4.1.16) \\
p^{\mathrm{st}}_2(X_2) &= \mathcal{N}_1(X_2; 0, (\mathbf{\Sigma}_\mathrm{b})_{22}) \\
&= \sqrt{\frac{\alpha(\alpha+3w_-)}{\pi\gamma^2(\alpha+w_-)}} \exp\left[-\frac{1}{\gamma^2}\frac{\alpha(\alpha+3w_-)}{\alpha+w_-}X_2^2\right], && (4.1.17) \\
p^{\mathrm{st}}_3(X_3) &= \mathcal{N}_1(X_3; 0, (\mathbf{\Sigma}_\mathrm{b})_{33}) \\
&= \sqrt{\frac{\alpha(\alpha+w_-)(\alpha+3w_-)}{\pi\gamma^2(\alpha^2+3\alpha w_-+w_-^2)}} \exp\left[-\frac{1}{\gamma^2}\frac{\alpha(\alpha+w_-)(\alpha+3w_-)}{\alpha^2+3\alpha w_-+w_-^2}X_3^2\right]. && (4.1.18)
\end{aligned}$$

where $(\mathbf{\Sigma}_b)_{ij}$ denotes the (i,j)-th entry of the covariance matrix $\mathbf{\Sigma}_\mathrm{b}$. Equations (4.1.16)–(4.1.18) align with numerical simulations, as shown in Fig. 4.1.5.

From Eqs. (4.1.14) and (4.1.5), the conditional correlation coefficients conditioned on $X_1 = \tilde{x}$, $X_2 = \tilde{x}$, $X_3 = \tilde{x}$ are respectively

$$\rho_{23|1} \equiv \rho(X_2, X_3 \mid X_1 = \tilde{x}) = \frac{w_-}{\sqrt{(\alpha+w_-)(\alpha+2w_-)}}, \tag{4.1.19}$$

$$\rho_{13|2} \equiv \rho(X_1, X_3 \mid X_2 = \tilde{x}) = 0, \tag{4.1.20}$$

$$\rho_{12|3} \equiv \rho(X_1, X_2 \mid X_3 = \tilde{x}) = \frac{w_-}{\sqrt{(\alpha+w_-)(\alpha+2w_-)}}. \tag{4.1.21}$$

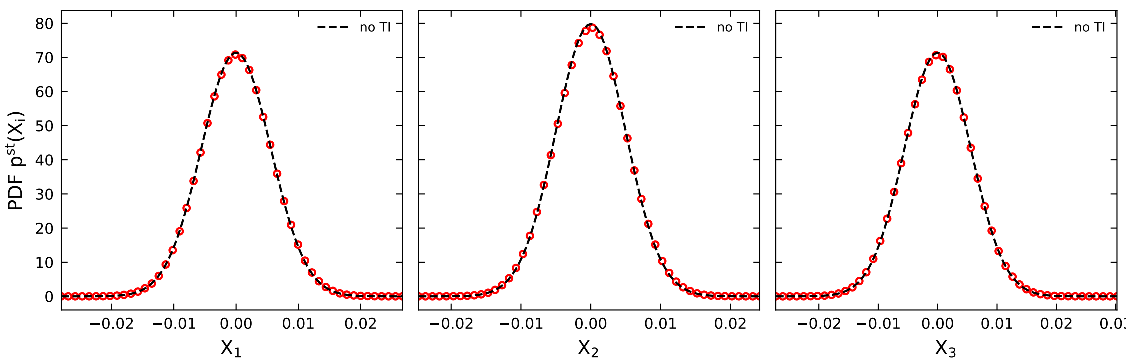

Figure 4.1.5: Stationary node state distribution of motif G_b without triadic interactions. The simulations are conducted with parameter values $w_- = 1$, $w_+ = 2$, $\alpha = 1$, $\hat{T} = 10^{-3}$, $\gamma = 10^{-2}$, $dt = 10^{-2}$, and $T_\mathrm{max} = 100$. The black dashed lines are the theoretical PDFs given by Eqs. (4.1.16)–(4.1.18), and the red open circles are the empirical marginal PDFs obtained from 10^3 realisations of the simulations. For each realisation, we extracted data from time range $[T_\mathrm{max}/2, T_\mathrm{max}]$. Empirical PDFs are obtained by binning the data points into 50 bins.

Figure 4.1.6 shows the conditional correlations $\rho_{23|1}(X_1)$, $\rho_{13|2}(X_2)$, and $\rho_{12|3}(X_3)$ from Eqs. (4.1.19)–(4.1.21) and the numerical values from 10^3 simulations of the node dynamics. The analytical and numerical results agree well, except for both ends of the conditional variables where the number of data points is small.

Finally, for motif G_c in Fig. 3.3.1(c) without triadic interactions, we can derive from Eq. (4.1.3) that the covariance matrix $\mathbf{\Sigma}_\mathrm{c}$ of G_c is given by

$$\mathbf{\Sigma}_\mathrm{c} = \frac{\gamma^2}{2\alpha(\alpha + 3w_-)} \begin{pmatrix} \alpha + w_- & w_- & w_- \\ w_- & \alpha + w_- & w_- \\ w_- & w_- & \alpha + w_- \end{pmatrix}. \tag{4.1.22}$$

As shown in Fig. 4.1.7, the analytical and numerical results are in agreement, implying that Eq. (4.1.22) is correct.

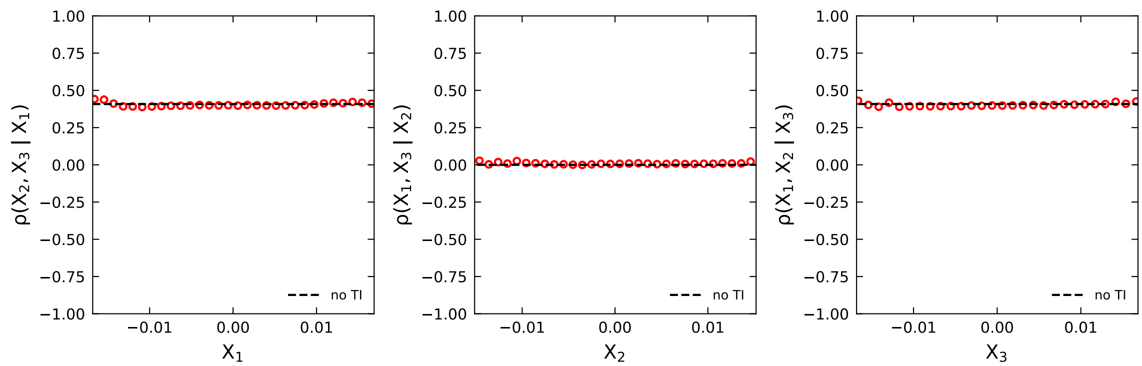

Figure 4.1.6: Conditional correlation coefficients in motif G_{b} without triadic interactions. The simulation parameters are set to $w_{-} = 1$, $w_{+} = 2$, $\alpha = 1$, $\hat{T} = 10^{-3}$, $\gamma = 10^{-2}$, $dt = 10^{-2}$, and $T_{\max} = 100$. The black dashed line is the theoretical conditional correlation given by Eq. (4.1.5), and the red open circles are the empirical conditional correlations obtained from 10^3 realisations of the simulations, where we extracted data points from time range $[T_{\max}/2, T_{\max}]$. Empirical conditional correlations are obtained by binning the data points into 50 bins. Due to the small sample size, the empirical conditional correlations fluctuate at both ends of the conditional variable, and thus we restrict the plotting range to $[-3\sigma_k, 3\sigma_k]$, where σ_k ($k \in \{1, 2, 3\}$) is the standard deviation of the conditional variable X_k.

From Eq. (4.1.1), the stationary solution of the joint PDF of node states in G_{c} is

$$
\begin{aligned}
&p_{123}^{\mathrm{st}}(X_1, X_2, X_3) = \mathcal{N}_3\left(X_1, X_2, X_3; 0, \boldsymbol{\Sigma}_{\mathrm{c}}\right) \\
&= \left(\frac{1}{\pi\gamma^2}\right)^{\frac{3}{2}} \sqrt{\alpha(\alpha + 3w_{-})^2} \\
&\qquad \times \exp\left[-\frac{1}{\gamma^2}\left\{(\alpha + 2w_{-})(X_1^2 + X_2^2 + X_3^2) - 2w_{-}(X_1X_2 + X_1X_3 + X_2X_3)\right\}\right].
\end{aligned} \tag{4.1.23}
$$

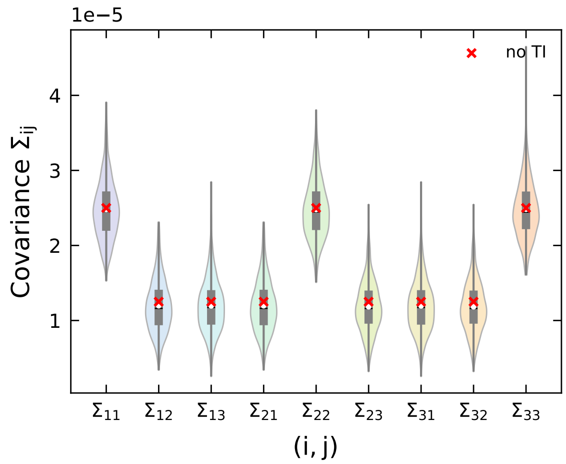

Figure 4.1.7: The covariance matrix $\mathbf{\Sigma}_\mathrm{c}$ of the network G_c without triadic interactions. The simulations are run with parameters $w_- = 1$, $w_+ = 2$, $\alpha = 1$, $\hat{T} = 10^{-3}$, $\gamma = 10^{-2}$, $dt = 10^{-2}$, and $T_\mathrm{max} = 100$. The ticks on the horizontal axis represent the entries in the covariance matrix. The distributions of numerically computed covariances from 10^3 realisations (with time range $[T_\mathrm{max}/2, T_\mathrm{max}]$) are shown as box plots with the median (black line) and the mean (white circle). The colour-filled curves are the kernel density estimates of the distributions. The red crosses indicate the theoretical values of the covariances in Eq. (4.1.22).

By applying Theorem 2.2.2, we obtain the marginal PDFs of X_1, X_2, and X_3 as

$$p_1^{\mathrm{st}}(X_1) = \mathcal{N}_1\left(X_1; 0, (\mathbf{\Sigma}_c)_{11}\right) = \sqrt{\frac{\alpha(\alpha+3w_-)}{\pi\gamma^2(\alpha+w_-)}} \exp\left[-\frac{1}{\gamma^2}\frac{\alpha(\alpha+3w_-)}{\alpha+w_-}X_1^2\right], \quad (4.1.24)$$

$$p_2^{\mathrm{st}}(X_2) = \mathcal{N}_1\left(X_2; 0, (\mathbf{\Sigma}_c)_{22}\right) = \sqrt{\frac{\alpha(\alpha+3w_-)}{\pi\gamma^2(\alpha+w_-)}} \exp\left[-\frac{1}{\gamma^2}\frac{\alpha(\alpha+3w_-)}{\alpha+w_-}X_2^2\right], \quad (4.1.25)$$

$$p_3^{\mathrm{st}}(X_3) = \mathcal{N}_1\left(X_3; 0, (\mathbf{\Sigma}_c)_{33}\right) = \sqrt{\frac{\alpha(\alpha+3w_-)}{\pi\gamma^2(\alpha+w_-)}} \exp\left[-\frac{1}{\gamma^2}\frac{\alpha(\alpha+3w_-)}{\alpha+w_-}X_3^2\right], \quad (4.1.26)$$

where $(\mathbf{\Sigma}_c)_{ij}$ denotes the (i,j)-th entry of the covariance matrix $\mathbf{\Sigma}_\mathrm{c}$. Equations (4.1.22) and (4.1.24)–(4.1.26) coincide with the numerical results as shown in Fig. 4.1.8.

From Eqs. (4.1.22) and (4.1.5), the conditional correlation coefficients conditioned

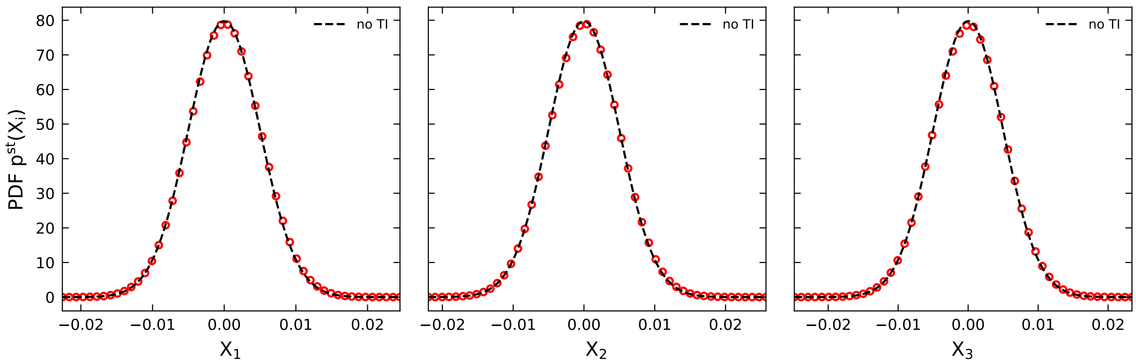

Figure 4.1.8: Stationary node state distribution of motif G_c without triadic interactions. The simulations are conducted with parameter values $w_- = 1$, $w_+ = 2$, $\alpha = 1$, $\hat{T} = 10^{-3}$, $\gamma = 10^{-2}$, $dt = 10^{-2}$, and $T_{\max} = 100$. The black dashed lines are the theoretical PDFs given by Eqs. (4.1.24)–(4.1.26), and the red open circles are the empirical marginal PDFs obtained from 10^3 realisations of the simulations. For each realisation, we extracted data from time range $[T_{\max}/2, T_{\max}]$. Empirical PDFs are obtained by binning the data points into 50 bins.

on $X_1 = \tilde{x}$, $X_2 = \tilde{x}$, $X_3 = \tilde{x}$ are respectively

$$\rho_{23|1} \equiv \rho(X_2, x_3 \mid X_1 = \tilde{x}) = \frac{w_-}{\alpha + 2w_-}, \tag{4.1.27}$$

$$\rho_{13|2} \equiv \rho(X_1, X_3 \mid X_2 = \tilde{x}) = \frac{w_-}{\alpha + 2w_-}, \tag{4.1.28}$$

$$\rho_{12|3} \equiv \rho(X_1, X_2 \mid X_3 = \tilde{x}) = \frac{w_-}{\alpha + 2w_-}. \tag{4.1.29}$$

Figure 4.1.9 shows the conditional correlations $\rho_{23|1}(X_1)$, $\rho_{13|2}(X_2)$, and $\rho_{12|3}(X_3)$ from Eqs. (4.1.11)–(4.1.13) and the numerical values from 10^3 simulations of the node dynamics. The analytical and numerical results agree well, except for both ends of the conditional variables, where the number of data points is small.

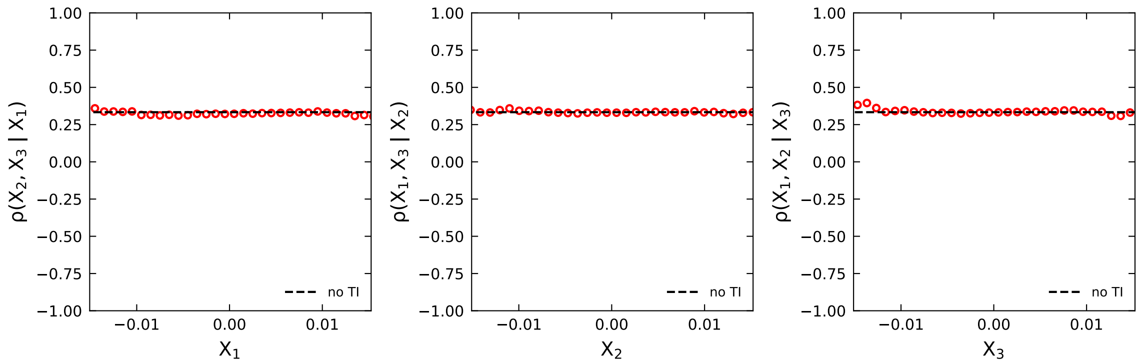

Figure 4.1.9: Conditional correlation coefficients in motif G_c without triadic interactions. The simulation parameters are set to $w_- = 1$, $w_+ = 2$, $\alpha = 1$, $\hat{T} = 10^{-3}$, $\gamma = 10^{-2}$, $dt = 10^{-2}$, and $T_{\max} = 100$. The black dashed line is the theoretical conditional correlation given by Eq. (4.1.5), and the red open circles are the empirical conditional correlations obtained from 10^3 realisations of the simulations, where we extracted data points from time range $[T_{\max}/2, T_{\max}]$. Empirical conditional correlations are obtained by binning the data points into 50 bins. Due to the small sample size, the empirical conditional correlations fluctuate at both ends of the conditional variable, and thus we restrict the plotting range to $[-3\sigma_k, 3\sigma_k]$, where σ_k ($k \in \{1, 2, 3\}$) is the standard deviation of the conditional variable X_k.

4.2 In the Prensence of Triadic Interactions

Based on the theory developed in Sect. 4.1, we now examine the effect of triadic interactions on the node dynamics in the presence of positive and negative regulators. We run simulations of the node dynamics (3.2.1) in the presence of positive and negative triadic interactions using the same parameter set as the numerical results presented in Sect. 4.1 for the three motif networks but without triadic interactions. The incidence matrices of positive and negative regulators in the three motif networks are presented in Eqs. (3.3.2), (3.3.3), and (3.3.4). The values of the node dynamics parameters are summarised in Table 4.1. We conducted 1000 independent realisations of the node dynamics for each motif network and each sign of triadic interaction, and computed the stationary node state distribution, covariances, and conditional correlation coefficients.

Table 4.1: Dynamics paramerter values in Sec. 4.3.

parameter	w_-	w_+	α	$\hat{T}$	γ	dt	$T_{\min}$	$T_{\max}$
value	1.0	2.0	1.0	10^{-3}	0.01	0.01	0.0	100.0

Figure 4.2.1 shows the marginal PDFs of node states in the presence of positive and negative triadic interactions. We observe that the signs of the triadic interactions do not affect the marginal PDFs of node states, as those for negative and positive triadic interactions are almost identical. In both cases, the marginal PDFs seem to follow Gaussian distributions, with the same mean and variance as those of the node dynamics in the absence of triadic interactions. In any case, we cannot observe consistent, notable differences between the marginal PDFs of node states with and without triadic interactions.

Next, we summarised the covariances in the presence of negative and positive regulators in Fig. 4.2.2. For all the cases, we notice a consistent trend that the diagonal elements of the covariance matrices decrease from the theoretic values in the absence of triadic interactions. This may indicate that the triadic interactions in our model decrease the variances of node states, which we could not observe clearly from the probability density functions presented in Fig. 4.2.1. Further exploration of the effect of triadic interactions on the variances of node states is conducted for more varied parameter sets, and the results were mixed. For some parameter sets, the variances of node states decrease, while for others, they remain the same as those of node dynamics in the absence of triadic interactions. The figures are not presented here due to the space limitation. Nevertheless, further investigation is required to understand the effect of triadic interactions on the variances of node states.

The most notable differences due to the triadic interactions are observed in the conditional correlation coefficients $\rho(X_i, X_j \mid X_k = \tilde{x})$, as shown in Fig. 4.2.3. While $\rho(X_i, X_j \mid X_k = \tilde{x})$ for any combination of i, j, and k is constant in the absence of triadic interactions, we observe the dependence on the conditional variable X_k when the triadic interaction is present. Our numerical results consistently show that $\rho(X_i, X_j \mid X_k = \tilde{x})$ transition from one value to another at a certain threshold value of $X_k = x_{\text{threshold}}$ when node k regulates the link connecting nodes i and j. One of the two values indeed corresponds to the value in the absence of triadic interactions. For $\rho(X_i, X_j \mid X_k = \tilde{x})$ in which node i (or j) regulates the link connecting nodes j (or i) and k, we observe a seemingly linear relationship between $\rho(X_i, X_j \mid X_k = \tilde{x})$ and X_k in motif G_a. Those in motif G_b and G_c are not linear, but waving around the value in the absence of triadic interactions. In any case, the conditional correlation coefficients in the presence of triadic interactions are not constant and show a non-trivial dependence on the conditional variable X_k. This result suggests that this dependence of the conditional correlation coefficients on the conditional variable X_k may be a signature of triadic interactions.

We notice that the value to which $\rho(X_2, X_3 \mid X_1 = \tilde{x})$ for motif G_a transitions from the value in the absence of triadic interaction is approximately equal to $w_+/(\alpha + w_+)$ (in Fig. 4.2.3, $w_+/(\alpha + w_+) = 2/3$ indicated by a black dotted line), which is the value of Eq. (4.1.11) in which w_- is replaced by w_+. Since node 1 in motif G_a only interacts with nodes 2 and 3 via triadic interactions, i.e., there are no edges connecting node 1 to nodes 2 and 3, the conditional correlation between X_2 and X_3 given X_1 is only determined by triadic interactions but with the alternative strength obtained from the switching of values in Eq. (3.2.3). Meanwhile, for motif G_b and G_c, the values of $\rho(X_2, X_3 \mid X_1 = \tilde{x})$ after transition are higher than the values of Eqs. (4.1.19) and (4.1.27) with w_+ in place for w_-. This is likely due to the correlation via the direct interaction of links from node 1 to nodes 2 and 3 in motif G_b and G_c and suggests that the triadic interactions can be harder to detect in the presence of direct interactions, i.e., links, because the effect of direct interactions will mix with the effect of triadic interactions. Nevertheless, the effect of triadic interactions is still observable in the conditional correlation coefficients, since the conditional correlation coefficients in the presence of triadic interactions clearly deviate from those in the absence of triadic interactions.

To further investigate the behaviours of conditional correlations in the presence of triadic interactions, we tested each parameter individually. The tested parameter sets are listed on Tab. 4.2. We primarily focus on the conditional correlation coefficients $\rho(X_2, X_3 \mid X_1 = \tilde{x})$, since it shows most notable differences from the case

Table 4.2: Dynamics parameter values.

	w_-	w_+	α	$\hat{T}$	γ	dt	$t_{\max}$
(R)	1.0	2.0	0.1	0.1	0.1	0.01	20.0
(A1)	0.1	0.2	0.1	0.1	0.1	0.01	20.0
(A2)	0.1	2.0	0.1	0.1	0.1	0.01	20.0
(A3)	1.0	20.0	0.1	0.1	0.1	0.01	20.0
(A4)	10.0	20.0	0.1	0.1	0.1	0.01	20.0
(B1)	1.0	2.0	0.01	0.1	0.1	0.01	20.0
(B2)	1.0	2.0	0.001	0.1	0.1	0.01	20.0
(C1)	1.0	2.0	0.1	-0.1	0.1	0.01	20.0
(C2)	1.0	2.0	0.1	0.01	0.1	0.01	20.0
(C3)	1.0	2.0	0.1	1.0	0.1	0.01	20.0
(D1)	1.0	2.0	0.1	0.1	0.01	0.01	20.0
(D2)	1.0	2.0	0.1	0.1	0.001	0.01	20.0

without triadic interactions. Furthermore, we only present the conditional correlation coefficient $\rho(X_2, X_3 \mid X_1 = \tilde{x})$ for motif G_{a} below, since the qualitative effects of each parameter are the same for the three motifs.

Figure 4.2.4 illustrates the w_- and w_+ depedence of conditional correlation coefficient $\rho(X_2, X_3 \mid X_1 = \tilde{x})$ conditioned on $X_1 = \tilde{x}$. From Fig. 4.2.4, we observe that the transition in $\rho(X_2, X_3 \mid X_1 = \tilde{x})$ appears most clearly when w_- and w_+ are well separated. Note, however, that we required $w_+ > w_- > 0$, and hence a larger w_+/w_- ratio is important for the observability of the transition in our model. Given a fixed ratio w_+/w_-, larger values of w_+ or w_- make the transition steeper.

The profiles of $\rho(X_2, X_3 \mid X_1 = \tilde{x})$ for varying values of α are shown in Fig. 4.2.5. While all the panels show step-like transitions in $\rho(X_2, X_3 \mid X_1 = \tilde{x})$, the larger value of α results in better profiles of $\rho(X_2, X_3 \mid X_1 = \tilde{x})$, with one value approximately equal to the theoretical value in the absence of triadic interactions. This is probably due to the faster convergence of the simulation for a larger value of α. When α is small, it takes longer to converge to its stationary state, and therefore it requires longer simulation time to obtain actual stationary solutions. However, we fixed the final time for all the parameter sets due to computational resource and time constraints. It should be evident from the plots of time evolution of the marginal PDFs of the variables that the simulations for smaller α are not stationary at the final time of the simulations.

The four panels in Fig. 4.2.6 illustate $\rho(X_2, X_3 \mid X_1 = \tilde{x})$ for four different values of the threshold parameter $\hat{T}$. From Fig. 4.2.6, we observe that the transitions in the values of $\rho(X_2, X_3 \mid X_1 = \tilde{x})$ occur at $X_k = \hat{T}$ (or its proximitiy). When $\hat{T} \gg 0$, we cannot observe the transition in $\rho(X_2, X_3 \mid X_1 = \tilde{x})$, because the triadic Laplacian never fluctuates as the value switching in $J_{ij}(\boldsymbol{X})$ of the model no longer happens. Indeed, $\rho(X_2, X_3 \mid X_1 = \tilde{x})$ in right, bottom panel (C3) is roughly constant at the theoretical value in the case with no triadic interactions. The fluctuation in the value of $\rho(X_2, X_3 \mid X_1 = \tilde{x})$ in (C3) is purely of stochastic nature, and should be flat when averaged over a sufficiently large number of simulations.

Finally, Fig. 4.2.7 demonstrates the γ-dependence of $\rho(X_2, X_3 \mid X_1 = \tilde{x})$. From our simulation results, we can conclude that the larger γ results in a more detectable transition in $\rho(X_2, X_3 \mid X_1 = \tilde{x})$, since we obtain a clearer profile of $\rho(X_2, X_3 \mid X_1 = \tilde{x})$. This makes sense for our model, since we require sufficiently large noises in the timeseries to detect correlations between node states, as the larger γ enables the nodes' timeseries to reflect correlations with other nodes stronger. In fact, in the limit of $\gamma \to 0$, we would have a completely deterministic dynamics and correlations cannot be measured in such a case.

4.3 Discussion

We examined the effects of triadic interactions on node states' timeseries data of our model dynamics by computing the conditional correlation coefficients $\rho(X_i, X_j \mid X_k = \tilde{x})$ for node tuples $(i, j, k) \in \mathcal{V}^3$ such that there exists at least one edge among the three nodes. Simulations support our theory that $\rho(X_i, X_j \mid X_k = \tilde{x})$ is constant if the random variables X_i, X_j, X_k interact only pairwise, that is, if there is no triadic interaction. When triadic interactions are introduced into networks, we observe non-trivial deviations in conditional correlation coefficients $\rho(X_i, X_j \mid X_k = \tilde{x})$ from constants. Specifically, in the case where node k interacts triadically with link $[i, j]$, the conditional correlation coefficient $\rho(X_i, X_j \mid X_k = \tilde{x})$ exhibits a transition in its values.

Our results also suggest that the detectability of triadic interactions depends on the structure of the underlying networks, the strength of interactions, and the noises in the timeseries data. In particular, we found that the detectability of triadic interactions is enhanced by increasing the strength w_+ of regulators and the noise amplitude γ. The threshold parameter $\hat{T}$ also plays an important role in the detection of triadic interactions for node dynamics, as the point at which transitions appear in $\rho(X_i, X_j \mid X_k = \tilde{x})$ is determined by $\hat{T}$.

The results of our model implies that the triadic interactions in real, multivariate timeseries data are likely detectable via the conditional correlation coefficients defined in Eq. (4.1.4) if the timeseries are stationary and sufficiently long and the triadic interactions are sufficiently stronger than pairwise interactions. Conditional correlation coefficients can be computed from the timeseries data without any prior knowledge of the underlying dynamics. Therefore, our method is applicable to a wide range of multivariate timeseries data, including those whose underlying dynamics are unknown. One significant limitation of our method is that we assume the underlying network structure of the dynamics to be known and that the dynamics of the network to depend on the triadic Laplacian. In cases where these assumptions are not valid, we may need to develop alternative models to comment on detectability.

It is important to note that the conditional correlation coefficients are not the only possible measures of triadic interactions. For example, we can also consider the conditional mutual information defined as

$$I(X_i; X_j | X_k = \tilde{x}) = \sum_{x_i \in X_i} \sum_{x_j \in X_j} p_{ij}(x_i, x_j \mid X_k = \tilde{x}) \ln \left[\frac{p_{ij}(x_i, x_j \mid X_k = \tilde{x})}{p_i(x_i \mid X_k = \tilde{x}) p_j(x_j \mid X_k = \tilde{x})} \right]. \tag{4.3.1}$$

It is of interest to investigate the detectability of triadic interactions via conditional mutual information as an extension to this work.

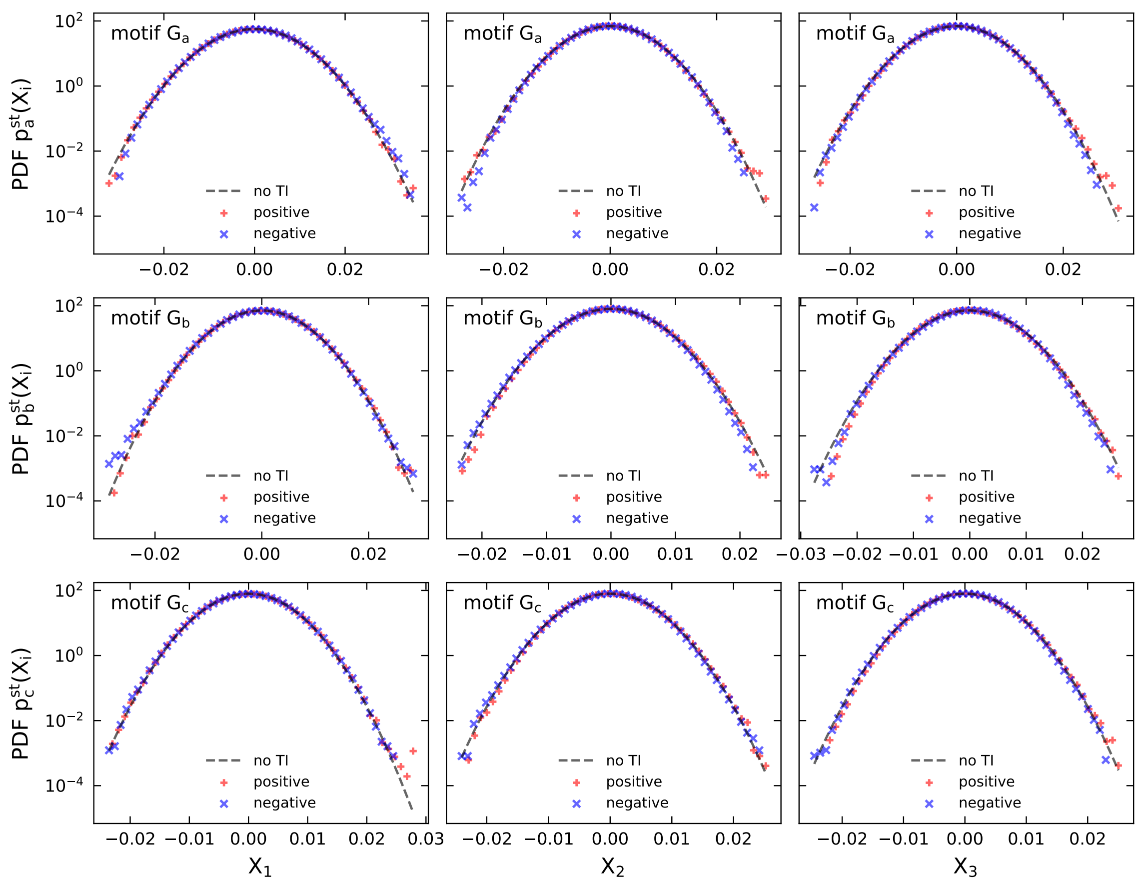

Figure 4.2.1: Probability density functions of node states in the presence of negative triadic interactions. Above, middle, and bottom rows correspond to motif (a), (b), and (c), while left, centre, and right panels in each row correspond to the marginal PDFs of node 1, 2, and 3, respectively. Red + and blue x markers indicate the numerically estimated marginal PDFs and the marginal PDFs of the motifs with positive and negative triadic interactions, respectively. Black dashed line in each panel is the theoretic marginal PDF for the node states in the absence of triadic interaction. The vertical axis is log-scaled.

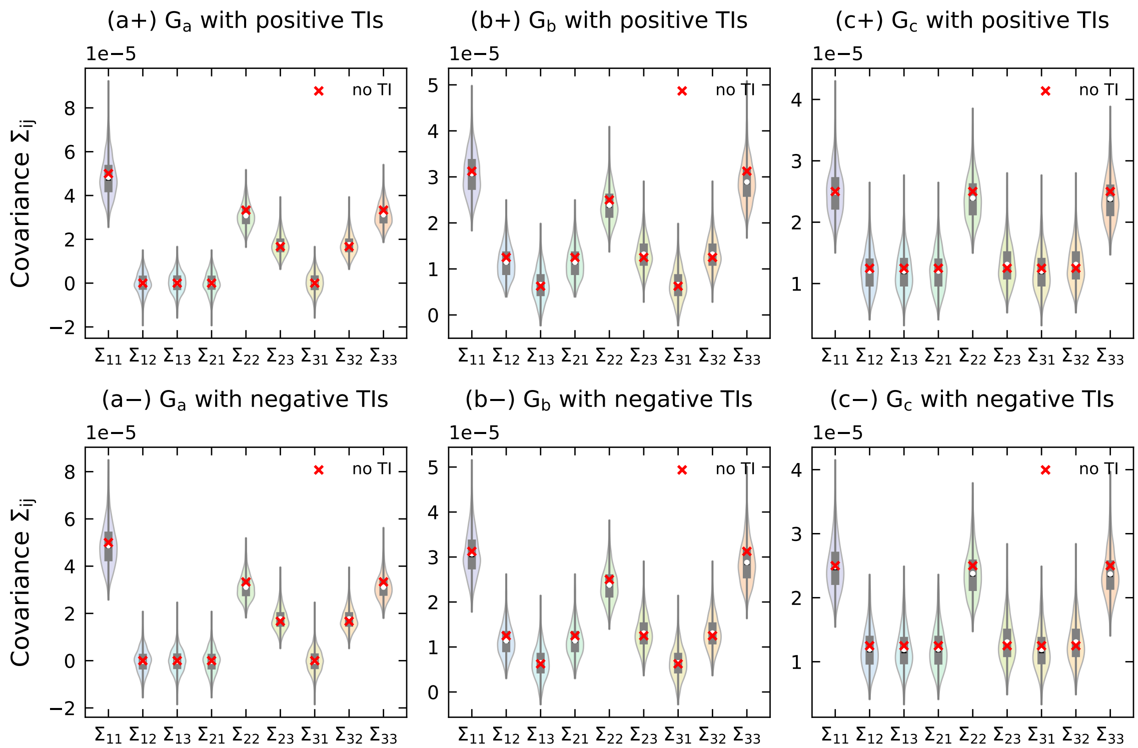

Figure 4.2.2: Covariances between pairs of node states in the presence of negative and positive triadic interactions. Top and bottom rows correspond to the covariances in the presence of negative and positive regulators, while left, centre, and right columns correspond to the motif (a), (b), and (c). The horizontal ticks correspond to the nine entries of the covariance matrix. White circles indicate the means of entries of the covariance matrix over 1000 simulations. Gray boxes and gray line segments illustrate the box plots of the distribution of entries of the covariance matrix over 1000 simulations. Violins (colour-filled curves) show the kernel density estimation of the distribution. Red crosses are theoretic predictions in the absence of triadic interactions.

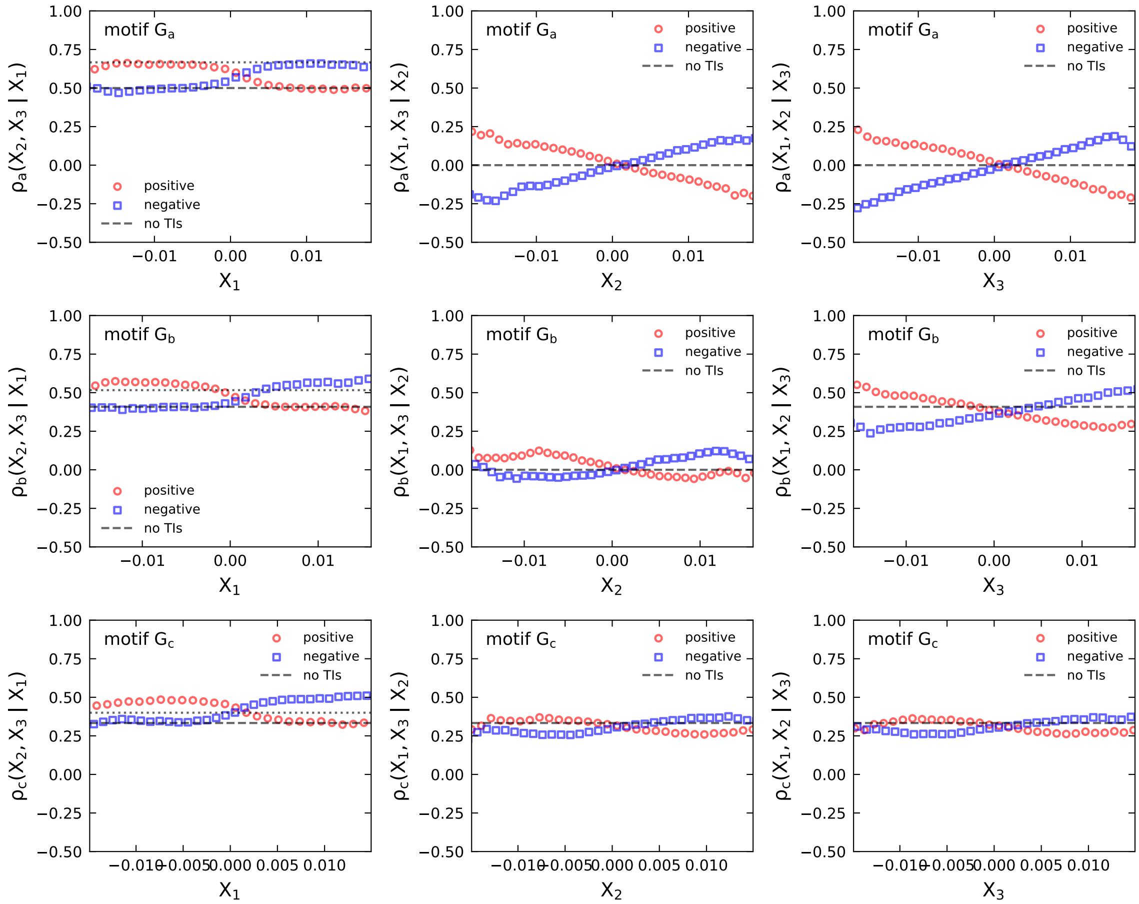

Figure 4.2.3: Conditional correlation coefficients of node states in the presence of positive and negative triadic interactions. Top, middle, and bottom rows correspond to motif (a), (b), and (c), while left, centre, and right columns correspond to conditional correlations conditioned on x_1, x_2, and x_3. In each panel, red open circles and blue open squares indicate the numerical results for the node dynamics with positive and negative triadic interactions, respectively. Black dashed line indicate the value in the absence of negative triadic interactions.

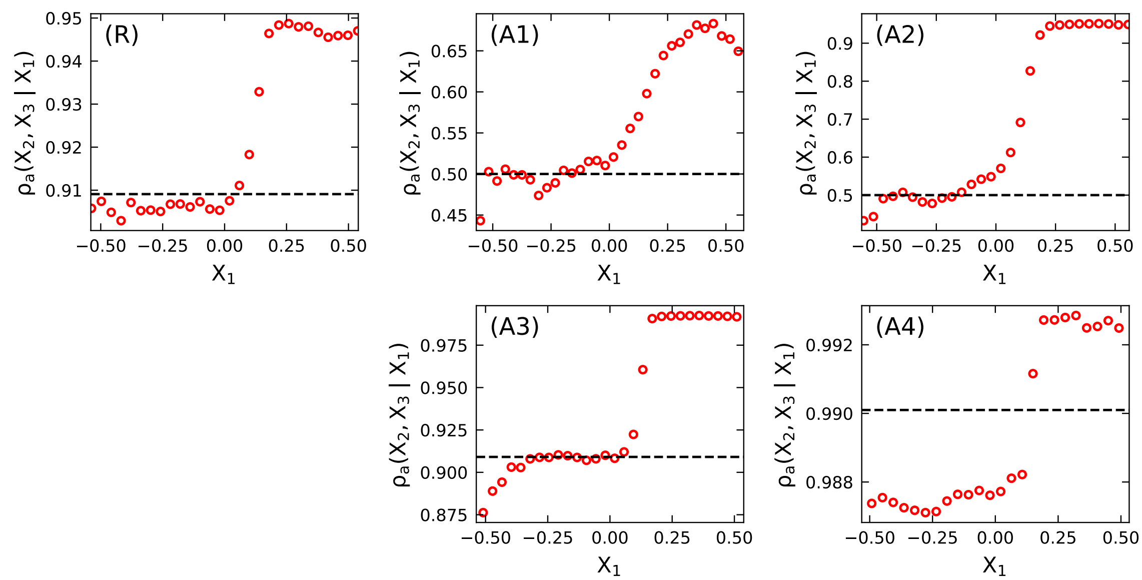

Figure 4.2.4: The w_-/w_+-depedence of conditional correlation coefficient $\rho(X_2, X_3 \mid X_1 = \tilde{x})$ in motif (a) with positive triadic interactions. Red open circles indicate the numerical results and black dashed line indicates the theoretical values in the absence of triadic interactions.

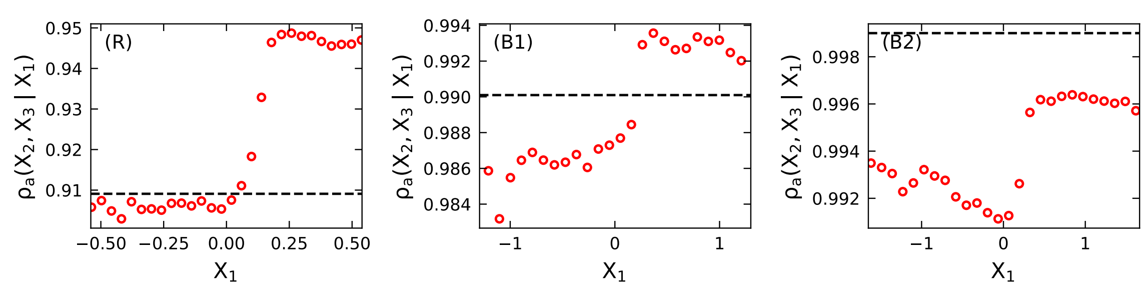

Figure 4.2.5: The α-depedence of conditional correlation coefficient $\rho(X_2, X_3 \mid X_1 = \tilde{x})$ in motif (a) with positive triadic interactions. Red open circles indicate the numerical results and black dashed line indicates the theoretical values in the absence of triadic interactions.

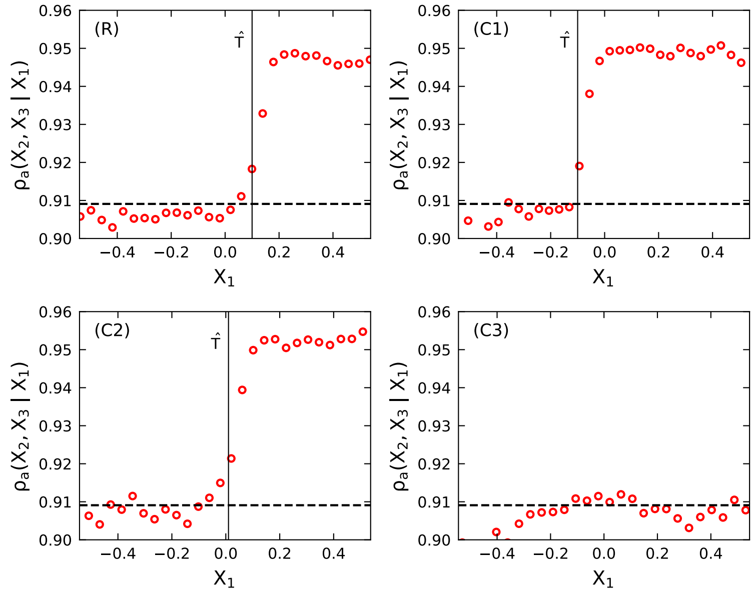

Figure 4.2.6: The $\hat{T}$-depedence of conditional correlation coefficient $\rho(X_2, X_3 \mid X_1 = \tilde{x})$ in motif (a) with positive triadic interactions. Red open circles indicate the numerical results and black dashed line indicates the theoretical values in the absence of triadic interactions. Vertical lines in panels (R), (C1), and (C2) show the values of $\hat{T}$.

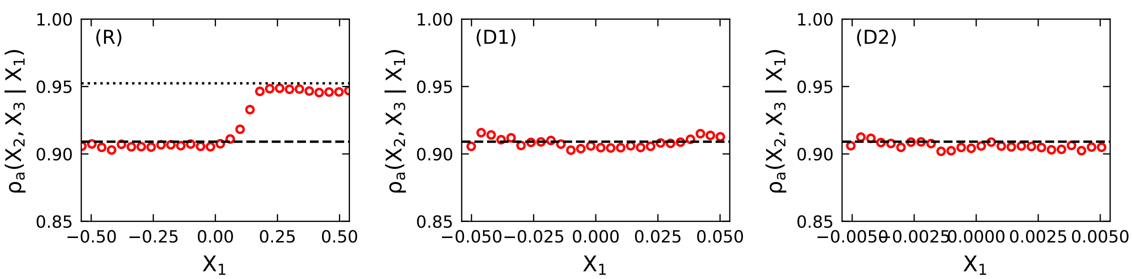

Figure 4.2.7: The γ-depedence of conditional correlation coefficient $\rho(X_2, X_3 \mid X_1 = \tilde{x})$ in motif (a) with positive triadic interactions. Red open circles indicate the numerical results and black dashed line indicates the theoretical values in the absence of triadic interactions. Dotted line in the left panel shows the value of Eq. (4.1.11) in which w_- replaced by w_+.

Chapter 5

Conclusion

In this study, we consider a node dynamics model that incorporates triadic interactions, where nodes in the network can interact positively or negatively with links. We examine how triadic interactions manifest themselves as conditional correlations between node states. We analytically solved for the stationary solution of the model when the triadic interactions are removed and showed that the stationary solution of the node dynamics is Gaussian distributed and that the conditional correlation coefficient is constant in the absence of the triadic interactions. These results were also confirmed by numerical calculations implemented in Python.

Numerical calculations were then performed for the case with triadic interactions, which could not be solved analytically, and compared with the analytical solution for the case without triadic interactions. It was confirmed that there were no apparent differences in the stationary distribution of the node states and the covariance matrix. On the other hand, it was found that the conditional correlation coefficients deviate non-trivially from those in the absence of triadic interactions. The effect of triadic interactions on the conditional correlations vary depending on the signs and strength of the triadic interaction. The results indicate the possibility of detecting the existence and signs of triadic interactions in real multivariate timeseries data through conditional correlation correlations.

For future prospects, verifying whether triadic interactions can be detected using conditional correlation coefficients in larger networks with more triadic interactions and in real multivariate time series data is essential. Further investigation into the potential changes in variance of the marginal node state distribution in the presence of triadic interactions is also necessary to properly assess the effects of triadic interactions. Finally, we need to examine whether it is possible to detect on the basis of conditional mutual information, since we could not fully summarise the results over the duration of this dissertation. We would like to continue our investigation into conditional mutual information as an alternative measure for triadic interactions.

Appendix A

Derivation of Stationary Node State Distribution

The incidence matrix of triadic interactions $\mathbf{K}$ in the absence of triadic interactions is given by

$$K_{\ell i} = 0, \quad \forall \ell \in \mathcal{E}, \forall i \in \mathcal{V}. \tag{A.1}$$

Equation (A.1) implies that for any node state $\boldsymbol{X} \in \mathbb{R}^N$ in the case of no triadic interactions,

$$\sum_{i=1}^{N} K_{\ell i} X_i = 0, \quad \forall \ell \in \mathcal{E}. \tag{A.2}$$

Without the loss of generality[1], suppose $\hat{T} > 0$. Then, from Eqs. (3.2.3) and (A.2), we have

$$J_{ij}(\boldsymbol{X}) = \begin{cases} w_- & \text{if } [i,j] \in \mathcal{E}, \\ 0 & \text{otherwise.} \end{cases} \tag{A.3}$$

[1] In case $\hat{T} < 0$, $J_{ij}(\boldsymbol{X}) = w_+$ if $[i,j] \in \mathcal{E}$ and 0 otherwise.

Using Eq. (3.2.2), this leads to the following triadic Laplacian:

$$\mathbf{L}^{(T)} = w_{-}\mathbf{L}, \tag{A.4}$$

where $\mathbf{L}$ is the Laplacian of the structural network G. When this is the case, the first term of Eq. (3.2.1) is the product of the constant matrix $w_{-}\mathbf{L} + \alpha\mathbf{I}$ and node state vector $\boldsymbol{X}$. This implies that Eq. (3.2.1) is equivalent to the SDE of the Ornstein-Uhlenbeck process (see Eq. (2.3.16)). Namely, Eq. (3.2.1) reads

$$d\boldsymbol{X}(t) = -\boldsymbol{A}\boldsymbol{X}(t)dt + \mathbf{B}d\boldsymbol{W}_t \tag{A.5}$$

where

$$\boldsymbol{A} = w_{-}\mathbf{L} + \alpha\mathbf{I}, \quad \mathbf{B} = \mathrm{diag}(\{\underbrace{\gamma, \ldots, \gamma}_{N}\}). \tag{A.6}$$

Hence, the stationary solution of the model in the absence of triadic interactions is given by

$$p_{\mathrm{st}}(\boldsymbol{X}) = \left(\frac{1}{\pi\gamma^2}\right)^{\frac{N}{2}} \sqrt{|w_{-}\mathbf{L} + \alpha\mathbf{I}|} \exp\left[-\frac{1}{\gamma^2}\boldsymbol{X}^{\top}\left(w_{-}\mathbf{L} + \alpha\mathbf{I}\right)\boldsymbol{X}\right], \tag{A.7}$$

which is a multivariate Gaussian distribution with mean $\mathbf{0}$ and covariance matrix $\boldsymbol{\Sigma}$ given by Eqs. (4.1.2) and (4.1.3), respectively. The precision matrix $\boldsymbol{\Lambda}$ is the inverse of the covariance matrix $\boldsymbol{\Sigma}$ and thus reads

$$\boldsymbol{\Lambda} := \boldsymbol{\Sigma}^{-1} = \frac{2}{\gamma^2}\left(w_{-}\mathbf{L} + \alpha\mathbf{I}\right). \tag{A.8}$$

Appendix B

Derivation of Conditional Correlations

Here, we present the derivations of the conditional correlation coefficients for the node dynamics in the absence of triadic interactions.

From Eq. (4.1.4), the conditional correlation coefficient of our interest can be expressed as

$$\rho(X_i, X_j \mid X_k = \tilde{x}) = \frac{\mathrm{Cov}\left[X_i,\ X_j \mid X_k = \tilde{x}\right]}{\sqrt{\mathrm{Var}\left[X_i \mid X_k = \tilde{x}\right]\mathrm{Var}\left[X_j \mid X_k = \tilde{x}\right]}}, \quad \tilde{x} \in \mathbb{R}. \tag{B.1}$$

Thus, to compute the conditional correlations, we require the conditional PDF $p_{ij|k}(X_i, X_j \mid X_k = \tilde{x})$ and its covariance matrix. We shall first take the marginal PDF $p_{ijk}(X_i, X_j, X_k)$ from the joint PDF $p(\boldsymbol{X})$ with $\boldsymbol{X} \in \mathbb{R}^N$. From Theorem 2.2.2, we have

$$p_{ijk}(X_i, X_j, X_k) = \mathcal{N}_3(X_i, X_j, X_k; \boldsymbol{\mu}_{ijk}, \boldsymbol{\Sigma}_{ijk}), \tag{B.2}$$

with mean vector and covariance matrix

$$\boldsymbol{\mu}_{ijk} = \begin{pmatrix} \mu_i \\ \mu_j \\ \mu_k \end{pmatrix} = \mathbf{0}, \quad \boldsymbol{\Sigma}_{ijk} = \begin{pmatrix} \Sigma_{ii} & \Sigma_{ij} & \Sigma_{ik} \\ \Sigma_{ji} & \Sigma_{jj} & \Sigma_{jk} \\ \Sigma_{ki} & \Sigma_{kj} & \Sigma_{kk} \end{pmatrix}. \tag{B.3}$$

Then, from Theorem 2.2.3, the conditional PDF $p_{ij|k}(X_i, X_j \mid X_k = \tilde{x})$ conditioned on $X_k = \tilde{x}$ reads

$$p_{ij|k}(X_i, X_j \mid X_k = \tilde{x}) = \mathcal{N}_2\left(X_i, X_j; \boldsymbol{\mu}_{ij|k}, \boldsymbol{\Sigma}_{ij|k}\right), \tag{B.4}$$

where

$$\boldsymbol{\mu}_{ij|k} = \begin{pmatrix} \mu_i \\ \mu_j \end{pmatrix} + \frac{\tilde{x} - \mu_k}{\Sigma_{kk}^2} \begin{pmatrix} \Sigma_{ik} \\ \Sigma_{jk} \end{pmatrix} = \frac{\tilde{x}}{\Sigma_{kk}^2} \begin{pmatrix} \Sigma_{ik} \\ \Sigma_{jk} \end{pmatrix}, \tag{B.5}$$

$$\boldsymbol{\Sigma}_{ij|k} = \begin{pmatrix} \Sigma_{ii} & \Sigma_{ij} \\ \Sigma_{ji} & \Sigma_{jj} \end{pmatrix} - \frac{1}{\Sigma_{kk}} \begin{pmatrix} \Sigma_{ik}\Sigma_{ki} & \Sigma_{ik}\Sigma_{kj} \\ \Sigma_{jk}\Sigma_{ki} & \Sigma_{jk}\Sigma_{kj} \end{pmatrix}. \tag{B.6}$$

It follows from Eq. (B.1) and (B.6) that

$$\rho(X_i, X_j \mid X_k = \tilde{x}) = \frac{\Sigma_{ij} - \Sigma_{kk}^{-1}\Sigma_{ik}\Sigma_{kj}}{\sqrt{(\Sigma_{ii} - \Sigma_{kk}^{-1}\Sigma_{ik}\Sigma_{ki})(\Sigma_{jj} - \Sigma_{kk}^{-1}\Sigma_{jk}\Sigma_{kj})}}, \quad \tilde{x} \in \mathbb{R}. \tag{B.7}$$

Appendix C

Overview of Python Implementations

We implemented Python source codes to run simulations of node dynamics on networks with the triadic interaction described in Chap. 3. Python scripts are available at github.com/jym16/node_dynamics_with_triadic_interactions. The scripts utilise the custom Python package `triadic_interaction` equipped with the following modules:

- `model.py`: the Python class for the node dynamics model (`NDwTIs`) is defined,
- `computation.py`: the functions to compute probability density function, covariance, and conditional correlation are defined,
- `visualization.py`: the functions to generate plots of our interests are written.

Inside the package, the Python library `sdeint` [Abu17] is used to solve the multivariate stochastic differential equation of our model. I also received assistance from Dr. Anthony Baptista in implementing the `create_node_edge_incidence_matrix` function in `computation.py` and the `NDwTIs` class in `model.py`. For further information, refer to the source codes and `readme.rst` in the repository.

Finally, we used Queen Mary's Apocrita HPC facility [Apo] to run the simulations.

Bibliography

[AB02] Réka Albert and Albert-László Barabási, *Statistical mechanics of complex networks*, Reviews of Modern Physics **74** (2002), no. 1, 47.

[Abu17] Matthew J. Aburn, *Critical fluctuations and coupling of stochastic neural mass models*, January 2017.

[Apo] This project utilised Queen Mary's Apocrita HPC facility, supported by QMUL Research-IT.

[BA99] Albert-László Barabási and Réka Albert, *Emergence of scaling in random networks*, Science **286** (1999), no. 5439, 509–512.

[BAB+21] Federico Battiston, Enrico Amico, Alain Barrat, Ginestra Bianconi, Guilherme Ferraz de Arruda, Benedetta Franceschiello, Iacopo Iacopini, Sonia Kéfi, Vito Latora, Yamir Moreno, Micah M. Murray, Tiago P. Peixoto, Francesco Vaccarino, and Giovanni Petri, *The physics of higher-order interactions in complex systems*, Nature Physics **17** (2021), no. 10, 1093–1098.

[BBC+14] Stefano Boccaletti, Ginestra Bianconi, Regino Criado, Charo I Del Genio, Jesús Gómez-Gardenes, Miguel Romance, Irene Sendina-Nadal, Zhen Wang, and Massimiliano Zanin, *The structure and dynamics of multilayer networks*, Physics Reports **544** (2014), no. 1, 1–122.

[BCI+20] Federico Battiston, Giulia Cencetti, Iacopo Iacopini, Vito Latora, Maxime Lucas, Alice Patania, Jean-Gabriel Young, and Giovanni

Petri, *Networks beyond pairwise interactions: Structure and dynamics*, Physics Reports **874** (2020), 1–92.

[Bia18] Ginestra Bianconi, *Multilayer networks: Structure and function*, Oxford University Press, 2018.

[Bia21] ______, *Higher-order networks: An introduction to simplicial complexes*, Cambridge University Press, 2021.

[BKK16] Eyal Bairey, Eric D Kelsic, and Roy Kishony, *High-order species interactions shape ecosystem diversity*, Nature Communications **7** (2016), no. 1, 12285.

[BLM+06] Stefano Boccaletti, Vito Latora, Yamir Moreno, Martin Chavez, and D-U Hwang, *Complex networks: Structure and dynamics*, Physics Reports **424** (2006), no. 4-5, 175–308.

[BN06] Christopher M Bishop and Nasser M Nasrabadi, *Pattern recognition and machine learning*, vol. 4, Springer, 2006.

[CBL16] Woo-Hyun Cho, Ellane Barcelon, and Sung Joong Lee, *Optogenetic glia manipulation: possibilities and future prospects*, Experimental Neurobiology **25** (2016), no. 5, 197.

[DGGNA19] Raissa M D'Souza, Jesus Gómez-Gardenes, Jan Nagler, and Alex Arenas, *Explosive phenomena in complex networks*, Advances in Physics **68** (2019), no. 3, 123–223.

[Gar09] Crispin Gardiner, *Stochastic methods: A handbook for the natural and social sciences*, vol. 4, Springer Berlin, 2009.

[GBMSA17] Jacopo Grilli, György Barabás, Matthew J Michalska-Smith, and Stefano Allesina, *Higher-order interactions stabilize dynamics in competitive network models*, Nature **548** (2017), no. 7666, 210–213.

[Hau16] Martin Haugh, *IEOR E4602: Quantitative risk management multivariate distributions*, Spring 2016.

[HS19] Petter Holme and Jari Saramäki, *Temporal network theory*, vol. 2, Springer, 2019.

[KAB+14] Mikko Kivelä, Alex Arenas, Marc Barthelemy, James P Gleeson, Yamir Moreno, and Mason A Porter, *Multilayer networks*, Journal of Complex Networks **2** (2014), no. 3, 203–271.

[LNR17] Vito Latora, Vincenzo Nicosia, and Giovanni Russo, *Complex networks: Principles, methods and applications*, Cambridge University Press, 2017.

[LS19] Andrew D Letten and Daniel B Stouffer, *The mechanistic basis for higher-order interactions and non-additivity in competitive communities*, Ecology Letters **22** (2019), no. 3, 423–436.

[Mau16] Pierre-André G. Maugis, *Event conditional correlation: Or how non-linear linear dependence can be*, 2016.

[ML16] Naoki Masuda and Renaud Lambiotte, *A guide to temporal networks*, World Scientific, 2016.

[New03] Mark Newman, *The structure and function of complex networks*, SIAM Review **45** (2003), no. 2, 167–256.

[New18] ———, *Networks*, Oxford University Press, 2018.

[Oks13] Bernt Oksendal, *Stochastic differential equations: An introduction with applications*, Springer Science & Business Media, 2013.

[PM13] Marzieh Parandehgheibi and Eytan Modiano, *Robustness of interdependent networks: The case of communication networks and the power grid*, 2013 IEEE Global Communications Conference, IEEE, 2013, pp. 2164–2169.

[RR96] Hannes Risken and Hannes Risken, *The Fokker-Planck equation: Methods of solution and applications*, Springer, 1996.

[Soc20] Joram Soch, *Multivariate normal distribution — statproofbook.github.io*, https://statproofbook.github.io/D/mvn, 22-01-2020, [Accessed 30-05-2023].

[SRKB23] Hanlin Sun, Filippo Radicchi, Jürgen Kurths, and Ginestra Bianconi, *The dynamic nature of percolation on networks with triadic interactions*, Nature Communications **14** (2023), no. 1, 1308.

[Ton90] Yung Liang Tong, *Fundamental properties and sampling distributions of the multivariate normal distribution*, Springer, 1990.

[VP19] Pat Vatiwutipong and Nattakorn Phewchean, *Alternative way to derive the distribution of the multivariate Ornstein–Uhlenbeck process*, Advances in Difference Equations **2019** (2019), no. 1, 1–7.